



Universiteit  
Leiden  
The Netherlands

## 4D-Flow MRI of aortic and valvular disease

Juffermans, J.F.

### Citation

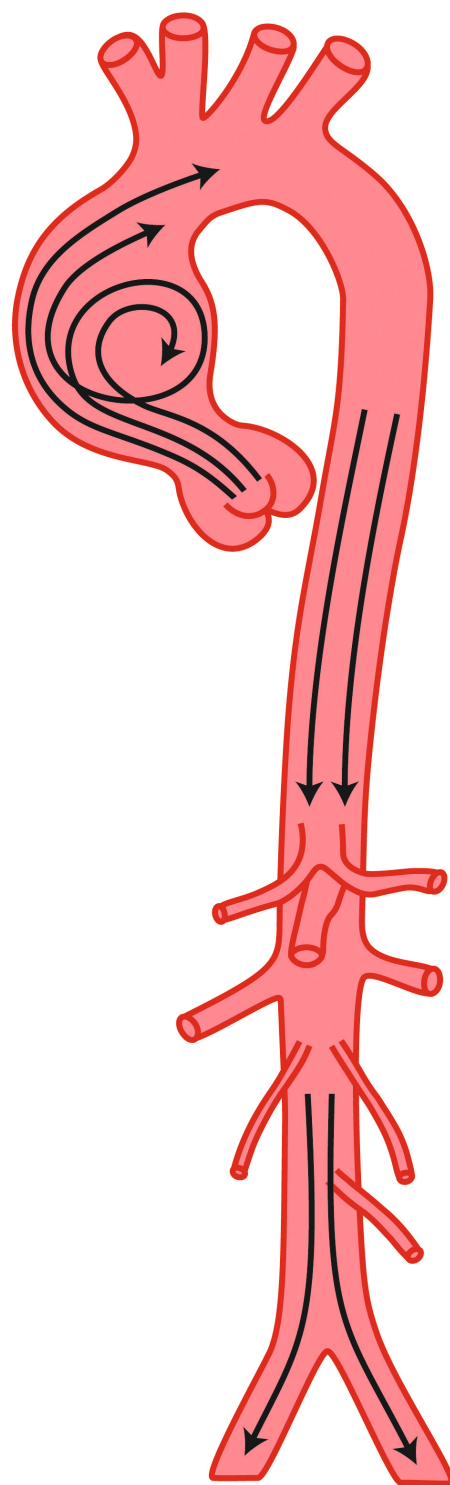
Juffermans, J. F. (2024, March 6). *4D-Flow MRI of aortic and valvular disease*. Retrieved from <https://hdl.handle.net/1887/3719932>

Version: Publisher's Version

[Licence agreement concerning inclusion of doctoral thesis in the Institutional Repository of the University of Leiden](#)

License: <https://hdl.handle.net/1887/3719932>

**Note:** To cite this publication please use the final published version (if applicable).



# CHAPTER 3

## 4D Flow MRI in Ascending Aortic Aneurysms: Reproducibility of Hemodynamic Parameters

---

*Joe F. Juffermans, Hans C. van Assen, Bastiaan J.C. te Kiefte, Mitch J. F.G. Ramaekers, Roel L.F. van de Palen, Pieter J. van den Boogaard, Bouke P. Adriaans, Joachim E. Wildberger,  
Arthur J.H.A. Scholte, Simon Schalla, Hildo J. Lamb, and Jos J. M. Westenberg.*

APPLIED SCIENCES, 2022, 12:8: 3912.

## ABSTRACT

**Background:** Aorta hemodynamics have been associated with aortic remodeling, but the reproducibility of its assessment has been evaluated marginally in patients with thoracic aortic aneurysm (TAA). The current study evaluated intra- and interobserver reproducibility of 4D flow MRI-derived hemodynamic parameters (normalized flow displacement, flow jet angle, wall shear stress (WSS) magnitude, axial WSS, circumferential WSS, WSS angle, vorticity, helicity, and local normalized helicity (LNH)) in TAA patients.

**Methods:** The thoracic aorta of 20 patients was semi-automatically segmented on 4D flow MRI data in 5 systolic phases by 3 different observers. Each time-dependent segmentation was manually improved and partitioned into six anatomical segments. The hemodynamic parameters were quantified per phase and segment. The coefficient of variation (COV) and intraclass correlation coefficient (ICC) were calculated.

**Results:** A total of 2400 lumen segments were analyzed. The mean aneurysm diameter was  $50.8 \pm 2.7$  mm. The intra- and interobserver analysis demonstrated a good reproducibility (COV = 16%–30% and ICC = 0.84–0.94) for normalized flow displacement and jet angle, a very good-to-excellent reproducibility (COV = 3%–26% and ICC = 0.87–1.00) for all WSS components, helicity and LNH, and an excellent reproducibility (COV = 3%–10% and ICC = 0.96–1.00) for vorticity.

**Conclusion:** 4D flow MRI-derived hemodynamic parameters are reproducible within the thoracic aorta in TAA patients.

## INTRODUCTION

Patients with a thoracic aortic aneurysm (TAA) have an increased risk for aortic rupture and dissection (1). Clinical guidelines use a maximal cross-sectional diameter  $\geq 55$  mm as the main criterion for the recommendation of preemptive surgical aortic replacement (2, 3). However, the majority (60%–96%) of dissections occur in aortas with diameters below this threshold (4, 5). Therefore, there is a need for additional and more sensitive markers to identify patients at high risk of progressive dilation or adverse aortic events (6).

Evaluation of aortic hemodynamics is considered to be highly promising for the prediction of progressive dilatation and adverse aortic events (7-14); the blood flow over the cardiac cycle through the aorta can be analyzed using three-dimensional time-resolved phase-contrast magnetic resonance imaging (MRI), also known as four-dimensional (4D) flow MRI. From 4D flow MRI data, several relevant patient-specific hemodynamic parameters can be assessed. It has been demonstrated for patients with a tricuspid aortic valve (TAV) that the amount of flow displacement (a measure of eccentricity in the flow profile) is associated with aortic growth (7, 8). Furthermore, TAV patients showed decreased levels of vortical flow, helical flow, and wall shear stress (WSS) compared to healthy volunteers (9, 10).

While such hemodynamic parameters could also be important for future clinical risk stratification of aneurysm patients, the majority of the studies assessing their agreements between observers and examinations only included healthy volunteers, patients with bicuspid aortic valves, or patients with mildly dilated aortas (13-22). Hence, the reported outcomes are not fully translatable to TAA patients with substantially dilated aortas and a TAV. Therefore, the reproducibility of the hemodynamic parameters in such patients remains unknown (1). Moreover, several previous studies quantified parameters based on (multiple) two-dimensional plane quantifications or ranked them qualitatively (15-18, 21). Thus, part of the spatial information is lost. In addition, the reproducibility of the WSS magnitude ( $WSS_{mag}$ ) has been assessed well, but little is known about the reproducibility of the axial or circumferential WSS component ( $WSS_{ax}$ ,  $WSS_{cir}$ , respectively) and the angle between both WSS components ( $WSS_{angle}$ ).

To allow quantification of hemodynamic parameters in 4D flow MRI data, a cardiac phase-specific 3D lumen segmentation is required (23, 24). The shape of these lumen segmentations can be described by morphologic parameters such as the volume, centerline length, maximal diameter, and curvature radius. Interestingly, a recent study demonstrated that the curvature radius of the ascending aorta is associated with aortic growth (7).

In most commercial and research software tools, these lumen segmentations are constructed (semi-)automatically on the 4D flow MRI data and then manually adjusted

when needed. The manual interaction may introduce observer-dependent variability in the quantitation of the hemodynamic parameters (25, 26). This observer-dependent variability of the 3D lumen segmentation can be assessed directly by evaluating the variability in morphologic parameters. The reproducibility of these morphologic parameters from 4D flow MRI data has been primarily reported in healthy volunteers (25).

Consequently, the aim of this study was to evaluate intra- and interobserver reproducibility of hemodynamic parameters, i.e., normalized flow displacement, flow jet angle, wall shear stress (magnitude, axial, circumferential, and angle), vorticity and helicity (absolute and local normalized) quantitatively assessed for six thoracic aortic lumen segments in patients with TAA and normally functioning TAV. In addition, intra- and interobserver reproducibility of morphological parameters, i.e., aortic volume, centerline length, lumen diameter, and curvature radius, were assessed.

## MATERIALS AND METHODS

### Study Population

The study protocol was conducted in accordance with the Declaration of Helsinki and was approved by the local Medical Ethics Committee of the Leiden University Medical Center (G20.149, 9 October 2020), which waived the patient's informed consent for anonymized clinical data. The clinical database was used to identify TAA patients with a TAV who underwent a 4D flow MRI of the thoracic aorta between October 2018 and August 2021 ( $n = 260$ ). Patients with aortic valve stenosis, regurgitation, or previous aortic surgery were excluded to obtain a selection of TAA patients without other pathologies, which potentially could also affect the reproducibility ( $n = 171$ ). The clinical reports of the patients were evaluated for the maximal aortic diameter, and the 20 patients with the largest reported maximal diameters were included, see Figure 1. The presence of an aortic root or ascending aorta aneurysm was classified according to Della Corte's classification (27).

### MRI Acquisition

The MRI examinations consisted of a 4D flow scan covering the entire thoracic aorta (for details, see Supplemental Table S1). All subjects were scanned with a 3T-scanner (Ingenia or Elition, Philips Healthcare, Best, The Netherlands) using a FlexCoverage anterior and dStream Torso posterior coil. Concomitant gradient correction was performed using standard available scanner software. All data were visually inspected, and the absence of aliasing in the 4D flow MRI data was confirmed.

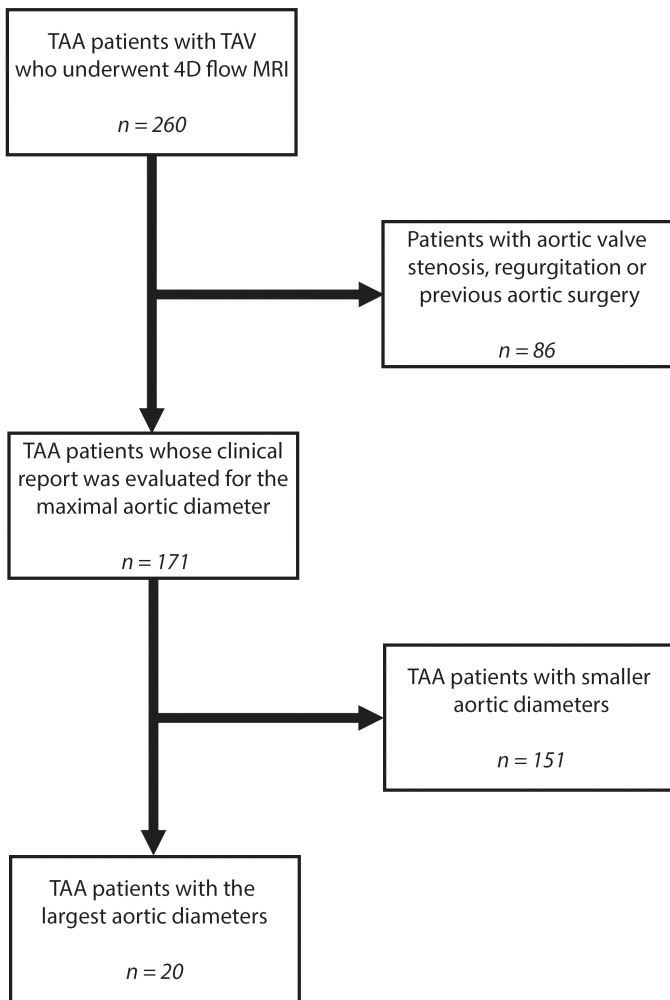


**Figure 1.** Population selection diagram. Abbreviations: TAA—thoracic aortic aneurysm, TAV—tricuspid aortic valve, MRI—magnetic resonance imaging, and 4D—four dimensional.

## Image Analysis

The image analysis consisted of three parts: 4D flow MRI lumen segmentation, aorta morphology quantification, and hemodynamic quantification. First, the aortic lumen of the patients was segmented twice by the first observer (J.J.) and once by the second and third observers (M.R. and B.K., respectively). Lumen segmentation was performed using CAAS MR Solutions v5.2.1 (Pie Medical Imaging, Maastricht, The Netherlands). The software generated initial segmentations on the peak systolic phase and two consecutive phases before and after this peak systolic phase (i.e., five systolic phases, see Figure 2). Next, the aortic segmentations were manually corrected for all five phases

and partitioned into six consecutive segments by manually placing anatomical planes perpendicular to the aortic centerline, respectively: the aortic root (from the aortic valve to the sinotubular junction), proximal ascending aorta (from the sinotubular junction to the mid-ascending aorta, defined as the midpoint on the centerline between the sinotubular junction and brachiocephalic artery), distal ascending aorta (from the mid-ascending aorta to the brachiocephalic artery), aortic arch (from the brachiocephalic artery until past the left subclavian artery), the proximal descending aorta (from the left subclavian artery to the mid-descending thoracic aorta, defined as the midpoint on the centerline between the left subclavian artery and the descending aorta at the level of the aortic valve), and distal descending aorta (from the mid-descending thoracic aorta to the descending aorta at the level of the aortic valve). More details about the aortic segmentation are described by van der Palen et al. (20). In addition, the stroke volume and cardiac output were assessed at the level of the sinotubular junction by the first observer for characterizing the left ventricular function of the population using CAAS MR Solutions.

Secondly, the morphology of the thoracic aortas was analyzed using an in-house developed Python software (Python Software Foundation, Wilmington, DE, USA). This tool was used to quantify aortic volume, centerline length, maximal diameter, and curvature radius of each anatomical segment and for each of the five systolic phases. The aortic diameter was determined by first constructing a cross-section perpendicular to the centerline at every millimeter. Next, at each cross-section, the maximal radial spike length was calculated. The curvature radius was derived by fitting a circle through the segments' centerline as previously described (25). The maximal aortic diameter within each segment and the radius of the fitted circle were used for statistical analysis.

Secondly, the morphology of the thoracic aortas was analyzed using an in-house developed Python software (Python Software Foundation, Wilmington, DE, USA). This tool was used to quantify aortic volume, centerline length, maximal diameter, and curvature radius of each anatomical segment and for each of the five systolic phases. The aortic diameter was determined by first constructing a cross-section perpendicular to the centerline at every millimeter. Next, at each cross-section, the maximal radial spike length was calculated. The curvature radius was derived by fitting a circle through the segments' centerline as previously described (25). The maximal aortic diameter within each segment and the radius of the fitted circle were used for statistical analysis.

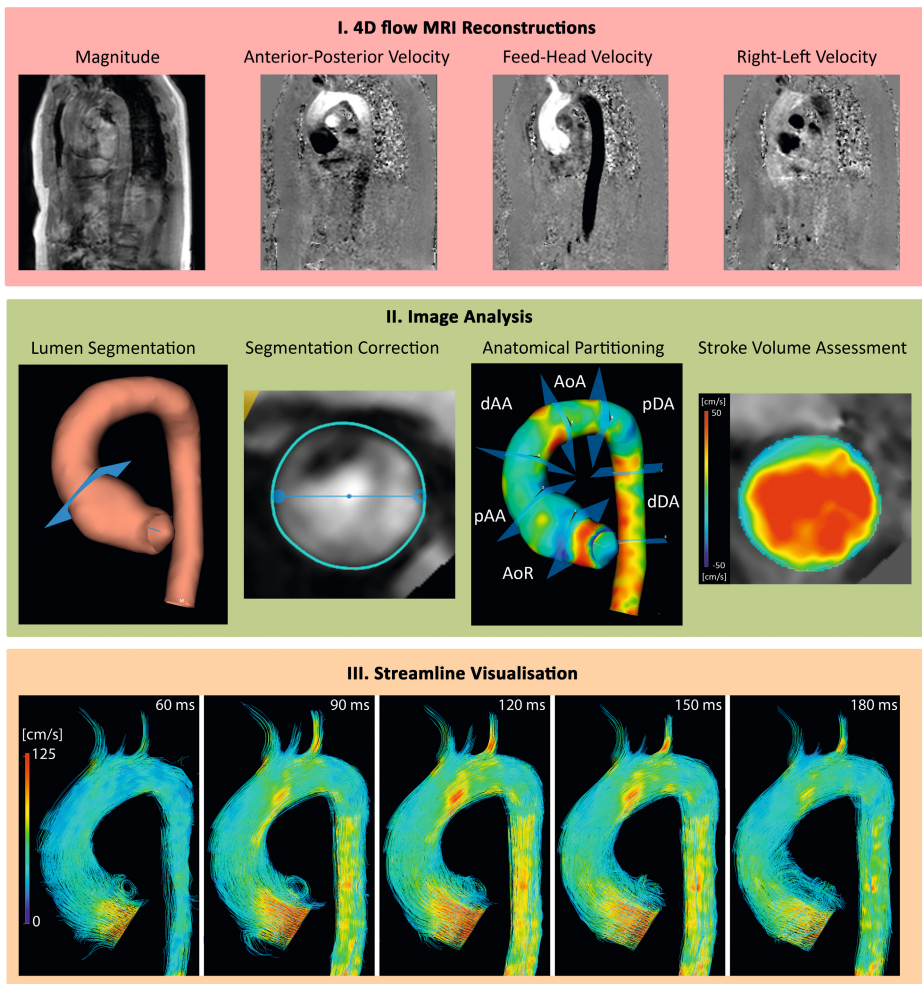


**Figure 2.** 4D flow MRI visualization using CAAS MR Solutions v.5.2.1. Example of a patient (male, 45 years old) with aortic root aneurysm with a diameter of 52 mm. (I) 4D flow MRI reconstructions. (II) Image analysis including the lumen segmentation, the manual segmentation correction, anatomical partitioning visualized on the wall shear stress maps, and Stroke volume assessment. (III) Streamline visualization of the 4D flow MRI at the 5 systolic phases (60, 90, 120, 150, and 180 ms). Abbreviations: AoR—aortic root, pAA—proximal ascending aorta, dAA—distal ascending aorta, AoA—aortic arch, pDA—proximal descending aorta, and dDA—distal descending aorta. Secondly, the morphology of the thoracic aortas was analyzed using an in-house developed Python software (Python Software Foundation, Wilmington, DE, USA). This tool was used to quantify aortic volume, centerline length, maximal diameter, and curvature radius of each anatomical segment and for each of the five systolic phases. The aortic diameter was determined by first constructing a cross-section perpendicular to the centerline at every millimeter. Next, at each cross-section, the maximal radial spike length was calculated. The curvature radius was derived by fitting a circle through the segments' centerline as previously described [25]. The maximal aortic diameter within each segment and the radius of the fitted circle were used for statistical analysis.

Thirdly, the hemodynamics of the thoracic aorta were quantified using methods described in previous studies (13, 15, 19). These methods were implemented in an in-house developed Python software (9, 25). Initially, the mean blood velocity over all subjects was quantified per anatomical segment. The tool was then used to quantify the normalized flow displacement, flow jet angle, vorticity norm, absolute helicity, and absolute LNH for each anatomical segment and each systolic phase. The normalized flow displacement and jet angle were determined by first constructing a cross-section perpendicular to the centerline at every millimeter. Next, at each cross-section, the normalized flow displacement (distance between the centerline point and center of velocity normalized for the vessel diameter times 100%) and flow jet angle (angle between the centerline and mean velocity vector) were calculated as previously described (15). The maximal normalized flow displacement and flow jet angle within each segment were assessed and used for statistical analysis. For the calculation of vorticity and helicity of the velocity vector fields ( $\vec{v}$ ), a spatial Gaussian differential operator ( $\vec{\nabla}$ ) with a standard deviation equal to the reconstructed in-plane voxel size was used. The vorticity ( $\vec{\omega} = \vec{\nabla} \times \vec{v}$ ) norm and absolute helicity ( $H = |\vec{v} \cdot \vec{\omega}|$ ) were quantified via methods previously described by Ramaekers et al. (9). The vorticity norm and absolute helicity were both normalized for the reconstructed voxel size, and the mean values within each segment were used for statistical analysis. Since a previous study demonstrated that a threshold of >0.6 for absolute LNH ( $LNH = \frac{|\vec{v} \cdot \vec{\omega}|}{|\vec{v}| |\vec{\omega}|}$ ) is the optimal criterion for detecting differences between patients and healthy volunteers (13), this threshold was used in our study to select volumes with increased absolute LNH. The volumes with increased absolute LNH were assessed and used for the statistical analysis. The in-house developed software can be made available for scientific collaboration per reasonable request. To derive 3D WSS maps for each of the five systolic phases, CAAS MR Solutions v5.2 was used. At each point of the 3D WSS map,  $WSS_{mag}$  was calculated as well as the  $WSS_{ax}$  and  $WSS_{cir}$  components. The  $WSS_{angle}$  between the  $WSS_{cir}$  and  $WSS_{ax}$  was quantified for each point as previously described (19). For each anatomical segment, the mean  $WSS_{mag}$ ,  $WSS_{ax}$ ,  $WSS_{cir}$ , and  $WSS_{angle}$  were used for statistical analysis.

## Observer Training

All observers were acquainted with CAAS MR Solutions software. The first, second, and third observer had 4, 3, and 1 years' experience with lumen segmentation on 4D flow MRI data in TAA patients, respectively. Since the observers were recruited at two clinical centers and observers had different levels of experience, all observers received feedback on the segmented aorta from an experienced cardiovascular MRI researcher (J.J.M.W. with >15 years of 4D flow MRI experience) after analyzing the training cohort ( $n = 10$  TAA patients). Hereafter, the results of the training cohort were not improved. Next, the observers analyzed the validation cohort ( $n = 10$  TAA patients).

## Statistical Analysis

Statistical analysis was performed using the open-source SciPy v1.2.1. software (28). Parametric and non-parametric data are expressed as mean  $\pm$  standard deviation (SD) or median (Q1–Q3), respectively. The Shapiro–Wilk test was used to verify the normality of the data. To assess the intra- and interobserver reproducibility, Bland–Altman analysis was performed, and the coefficient of variation (COV), Spearman rank correlation coefficient ( $r$ ), and intraclass correlation coefficient (ICC) (two-way mixed effects, absolute agreement) were calculated. For the Bland–Altman analysis, the mean difference and limits of agreement ( $LoA = 1.96 \times SD$ ) were computed (29). In addition, the relative difference in LoA between the training and validation cohort was calculated ( $LoA_{diff} = ((\text{validation } LoA - \text{training } LoA) / \text{training } LoA) \times 100\%$ ). The COV was classified as low ( $\leq 10\%$ ), intermediate (11%–20%), high (21%–30%), or very high ( $> 30\%$ ). The  $r$  and ICC were classified as poor ( $< 0.50$ ), moderate (0.50–0.69), good (0.70–0.84), very good (0.85–0.94), or excellent ( $\geq 0.95$ ) (25). A  $p$ -value of  $< 0.05$  was considered statistically significant.

## RESULTS

The patient characteristics are presented in Table 1. In Table 2, median values of hemodynamic and morphologic parameters are presented. Of the selected TAA patients, 13 presented with an aneurysm in the aortic root and 7 with an ascending aorta aneurysm. The mean TAA diameter and mean blood velocity were  $50.8 \pm 2.7$  mm and  $42.5 \pm 14.9$  cm·s $^{-1}$ , respectively.

A total of 2400 aorta segments were analyzed for the intra- and interobserver reproducibility analysis, see Figure 3. The result of these analyses over all anatomical segments and systolic phases for the validation and training cohort are presented in Table 3 and Supplemental Table S2, respectively.

Intra- and interobserver analysis of the hemodynamic parameters demonstrated a good reproducibility in the validation cohort for normalized flow displacement and flow jet angle ( $LoA \leq 4.8\%$  and  $\leq 8.7^\circ$  respectively, COV = 16%–32%,  $r = 0.70$ –0.92, ICC = 0.80–0.94), an excellent reproducibility for vorticity norm ( $LoA \leq 2779$  s $^{-1}$ ·mL $^{-1}$ , COV = 3%–10%,  $r = 0.96$ –1.00, ICC = 0.96–1.00), and a very good reproducibility for absolute WSS<sub>mag</sub>, WSS<sub>ax</sub>, WSS<sub>cir</sub>, WSS<sub>angle</sub>, absolute helicity and volumes with increased absolute LNH ( $LoA \leq 242$  mPa,  $\leq 244$  mPa,  $\leq 103$  mPa,  $\leq 8.9^\circ$ ,  $\leq 631$  m·s $^{-2}$ ·mL $^{-1}$  and  $\leq 8.4$  mL, respectively; COV = 3%–26%,  $r = 0.86$ –1.00, ICC = 0.86–1.00). See Supplemental Figures S1–S9 for the corresponding Bland–Altman plots. These plots demonstrated no striking dependency of the measured differences relative to the mean for the analyses and hemodynamic parameters.

Intra- and interobserver analysis of the morphologic parameters demonstrated a very good reproducibility in the validation cohort for volume and centerline length ( $LoA \leq 15.7$  mL and  $\leq 12.2$  mm, respectively; COV = 8%–22%,  $r = 0.89$ –0.98, ICC = 0.90–0.98),

and an excellent reproducibility for diameter ( $\text{LoA} \leq 5.0 \text{ mm}$ ,  $\text{COV} = 3\%–7\%$ ,  $r = 0.98–0.99$ ,  $\text{ICC} = 0.96–0.99$ ) and a good reproducibility for curvature radius ( $\text{LoA} \leq 46.4 \text{ mm}$ ,  $\text{COV} = 21\%–35\%$ ,  $r = 0.72–0.87$ ,  $\text{ICC} = 0.90–0.92$ ). See Supplemental Figures S10–S13 for the corresponding Bland–Altman plots. These plots demonstrated no dependency of the measured differences relative to the mean for most analyses and morphologic parameters, except for the maximal diameter, which had a slightly increasing difference relative to the mean for the interobserver analyses.

The intra- and interobserver reproducibility results per anatomical segment are presented in Supplemental Tables S3 and S4, respectively. The intra- and interobserver analysis showed for the validation cohort a similar reproducibility for most morphologic and hemodynamic parameters per segment. However, the reproducibility was slightly decreased within the aortic root for several parameters (i.e., flow displacement,  $\text{WSS}_{\text{mag}}$ ,  $\text{WSS}_{\text{ax}}$ , absolute helicity, volumes with increased absolute LNH, aortic segment volume, centerline length, and curvature radius). Furthermore, the reproducibility of the maximal diameter was slightly decreased within the proximal part of the aorta (i.e., the aortic root, proximal and distal ascending aorta) compared to the other anatomical segments further distally to the ascending aorta (intraobserver  $\text{LoA} \leq 2.7$  and  $\leq 1.8 \text{ mm}$ ; interobserver  $\text{LoA} \leq 7.6$  and  $\leq 3.3 \text{ mm}$ , respectively). Moreover, the reproducibility of  $\text{WSS}_{\text{angle}}$  was slightly decreased within the proximal and distal descending aorta.

Compared to the training cohort, the validation cohort demonstrated reduced LoA over all analyses for morphologic and hemodynamic parameters ( $\text{LoA}_{\text{diff}} = -12 [-26–3]\%$ ). This improvement was more evident for the morphologic parameters compared to the hemodynamic parameters ( $\text{LoA}_{\text{diff}} = -20 [-41–6]\%$  and  $-9 [-21–5]\%$ , respectively). Moreover, this improvement was also more evident within the aortic root, proximal and distal ascending aorta compared to the aortic arch, proximal and distal descending aorta ( $\text{LoA}_{\text{diff}} = -10 [-35–11]\%$  and  $2 [-18–41]\%$ , respectively).

**Table 1.** Population characteristics.

Characteristic	Quantity
Population size	20
Male (%)	18 (90%)
Age (years)	53 ± 14
Height (cm)	186 ± 8
Weight (kg)	90 ± 11
TAA diameter (mm)	50.8 ± 2.7
Heart rate (bpm)	68 ± 11
Stroke Volume (mL)	105 ± 24
Cardiac Output (L·min <sup>-1</sup> )	7.0 ± 1.8
Systolic blood pressure (mm Hg)	132 ± 14
Diastolic blood pressure (mm Hg)	81 ± 7
Trigger delay peak systole—2 phases (ms)	102 ± 31
Trigger delay peak systole—1 phase (ms)	133 ± 32
Trigger delay peak systole (ms)	163 ± 34
Trigger delay peak systole + 1 phase (ms)	194 ± 35
Trigger delay peak systole + 2 phases (ms)	224 ± 36

Data noted as the mean ± standard deviation and presented over all subjects. Abbreviation: TAA—thoracic aortic aneurysm.

**Table 2.** The hemodynamic and morphologic characteristics assessed in the thoracic aorta.

Parameter	Anatomical Segments					dDA
	AoR	pAA	dAA	AoA	pDA	
Flow Displacement (%)	7.5 (5.3–10.2)	9.8 (7.1–16.2)	6.3 (4.9–9.0)	5.7 (4.7–6.5)	6.5 (5.8–7.6)	4.7 (4.1–5.7)
Flow Jet Angle (°)	17.6 (13.7–21.9)	17.6 (11.9–27.0)	14.8 (10.2–21.3)	14.6 (12.5–17.3)	15.7 (13.1–18.4)	9.1 (7.6–10.6)
WSS magnitude (mPa)	561 (483–654)	763 (570–896)	750 (595–955)	746 (560–992)	877 (706–1,112)	939 (785–1,179)
Axial WSS (mPa)	371.9 (335–478)	627.9 (432–734)	702.6 (551–893)	700.6 (525–949)	801.5 (670–1,045)	915.2 (748–1,145)
Circumferential WSS (mPa)	331 (286–410)	331 (247–405)	204 (159–262)	182 (153–215)	243 (180–296)	205 (147–244)
WSS angle (°)	42.5 (37.4–45.7)	32.0 (26.8–37.1)	18.3 (13.7–24.0)	14.0 (12.1–16.9)	16.8 (14.4–20.2)	11.7 (9.6–14.4)
Vorticity Norm (s <sup>-1</sup> ·mL <sup>-1</sup> )	18,882 (16,767–21,131)	12,909 (10,629–15,526)	10,390 (7,695–12,407)	11,338 (9,273–14,205)	14,422 (11,800–19,372)	14,150 (11,164–17,990)
Absolute Helicity (m <sup>3</sup> ·s <sup>-2</sup> ·mL <sup>-1</sup> )	3,084 (2,327–3,603)	1,997 (1,287–2,729)	1,098 (624–1,544)	1,207 (950–1,749)	1,873 (1,149–2990)	1,464 (1,059–2,263)
Absolute Local Normalized Helicity Volume (mL)	19.4 (10.5–27.3)	24.8 (18.9–30.2)	15.2 (10.4–21.7)	9.4 (7.0–13.6)	15.6 (12.2–18.2)	17.7 (13.7–19.6)
Volume (mL)	44.1 (25.2–59.8)	53.2 (36.9–59.7)	41.1 (31.0–53.8)	28.6 (20.0–31.5)	38.4 (29.9–45.2)	31.5 (24.2–38.0)
Centerline Length (mm)	31.0 (24.3–37.1)	40.8 (36.6–44.0)	40.0 (36.7–44.3)	37.3 (34.0–38.7)	65.4 (57.0–69.2)	64.1 (58.0–68.9)
Maximal Diameter (mm)	48.7 (40.0–51.3)	44.7 (40.4–46.6)	41.2 (35.4–44.9)	34.3 (31.5–36.3)	31.3 (28.2–32.6)	27.3 (24.9–29.7)
Curvature Radius (mm)	51.4 (42.9–71.1)	38.5 (36.2–46.6)	50.6 (43.3–61.3)	46.1 (40.8–59.7)	45.5 (37.3–53.7)	38.1 (102.0–164.5)

Data noted as the median (Q1–Q3) and presented over all subject and systolic phases. Abbreviations: AoR—aortic root, pAA—proximal ascending aorta, dAA—distal ascending aorta, AoF—aortic arch, pDA—proximal descending aorta, and dDA—distal descending aorta.

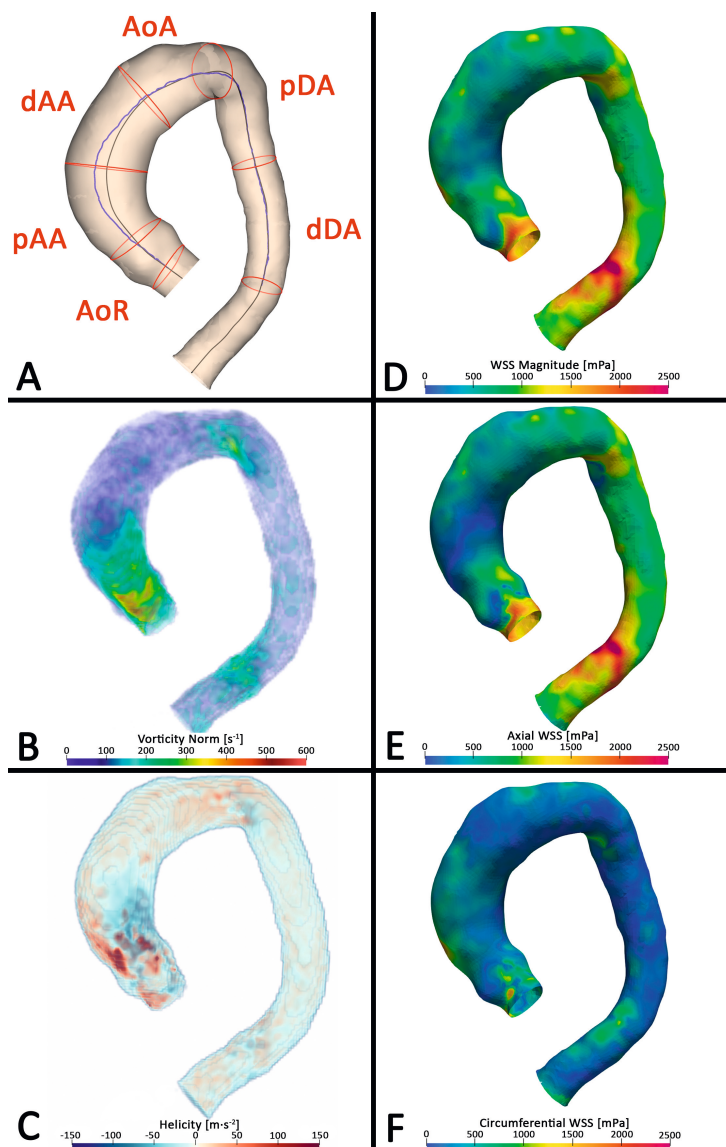


**Figure 3.** Aortic segments and hemodynamic parameters. Example of a patient (male, 71 years old) with an ascending aorta aneurysm with a diameter of 48 mm. (A) Anatomical segments with centerline (black color) and flow displacement line (blue color). (B) Vorticity norm. (C) Absolute helicity. Positive and negative magnitudes indicate a clockwise and anti-clockwise rotation, respectively. (D) Wall shear stress magnitude. (E) Axial wall shear stress. (F) Circumferential wall shear stress. Abbreviations: AoR—aortic root, pAA—proximal ascending aorta, dAA—distal ascending aorta, AoR—aortic arch, pDA—proximal descending aorta, dDA—distal descending aorta, and WSS—wall shear stress.

**Table 3.** Intra- and interobserver reproducibility: results of the validation cohort.

Study	Bland–Altman		Spearman Rank Correlation Coefficient		Intraclass Correlation Coefficient	LoA <sub>diff</sub> (%)
	Mean Diff	LoA	COV (%)			
Flow Displacement (%)						
IA-0	-0.1	2.8	19	0.81	0.94	-9
IE-01	-0.5	4.8	32	0.70	0.84	15
IE-02	0.1	4.4	30	0.70	0.85	3
IE-03	0.6	4.1	27	0.79	0.87	7
Flow Jet Angle (°)						
IA-0	0.3	5.0	16	0.92	0.93	-16
IE-01	-0.3	8.0	25	0.80	0.83	-4
IE-02	0.2	7.1	23	0.85	0.86	-9
IE-03	0.5	8.7	27	0.78	0.80	-4
WSS Magnitude (mPa)						
IA-0	0	43	3	1.00	1.00	-15
IE-01	-33	232	14	0.90	0.93	-10
IE-02	17	161	10	0.93	0.97	-25
IE-03	50	242	15	0.89	0.93	30
Axial WSS (mPa)						
IA-0	-0	47	3	1.00	1.00	-59
IE-01	-30	240	16	0.92	0.94	-58
IE-02	19	163	11	0.95	0.97	-51
IE-03	49	244	17	0.92	0.94	51
Circumferential WSS (mPa)						
IA-0	-1	39	8	0.98	0.98	11
IE-01	0	96	19	0.89	0.87	-18
IE-02	3	73	15	0.93	0.93	0
IE-03	3	103	20	0.86	0.87	-23
WSS Angle (°)						
IA-0	0.1	3.3	7	0.99	0.99	-47
IE-01	0.2	8.9	19	0.89	0.94	-8
IE-02	-0.7	7.5	16	0.95	0.96	-21
IE-03	-0.9	8.7	18	0.91	0.95	5
Vorticity Norm ( $s^{-1} \cdot mL^{-1}$ )						
IA-0	37	860	3	1.00	1.00	-40
IE-01	180	2,001	7	0.97	0.98	-4
IE-02	93	2,485	9	0.96	0.97	-22
IE-03	-87	2,779	10	0.96	0.96	6

**Table 3.** *Continued*

Study	Bland–Altman			Spearman Rank Correlation Coefficient	Intraclass Correlation Coefficient	LoA <sub>diff</sub> (%)
	Mean Diff	LoA	COV (%)			
Absolute Helicity ( $m \cdot s^{-2} \cdot mL^{-1}$ )						
IA-0	30	223	6	1.00	1.00	-9
IE-01	-16	394	10	0.98	0.98	14
IE-02	17	603	15	0.96	0.96	-14
IE-03	32	631	16	0.96	0.96	21
Absolute Local Normalized Helicity Volume (mL)						
IA-0	0.0	3.3	10	0.99	0.98	-18
IE-01	0.2	5.9	18	0.95	0.92	6
IE-02	0.9	8.4	26	0.88	0.86	-28
IE-03	0.7	6.3	20	0.92	0.91	-10
Volume (mL)						
IA-0	0.2	6.8	9	0.98	0.98	4
IE-01	1.0	12.7	18	0.93	0.90	-21
IE-02	1.9	15.7	22	0.89	0.86	-13
IE-03	0.9	10.8	15	0.94	0.92	-41
Centerline Length (mm)						
IA-0	0.9	7.1	8	0.94	0.97	-7
IE-01	0.2	11.9	14	0.90	0.92	-36
IE-02	3.5	12.2	14	0.89	0.92	-20
IE-03	3.3	8.0	9	0.94	0.96	-53
Maximal Diameter (mm)						
IA-0	-0.2	1.9	3	0.99	0.99	-14
IE-01	-0.0	4.0	6	0.98	0.97	-3
IE-02	-0.9	5.0	7	0.98	0.96	-42
IE-03	-0.9	4.3	6	0.98	0.97	-36
Curvature Radius (mm)						
IA-0	2.3	37.2	29	0.87	0.92	30
IE-01	-2.7	46.4	35	0.77	0.90	14
IE-02	3.6	42.4	34	0.77	0.90	-72
IE-03	6.3	43.5	34	0.72	0.92	-70

Characteristics are presented per cohort over all subjects, anatomical segments, and systolic phases ( $n = 300$ ). \* All probability values  $<0.01$ . Abbreviations: Mean Diff—mean difference; LoA—limits of agreement ( $1.96 \times$  standard deviation); COV—coefficient of variation; IA-0—intraobserver analysis by the first observer with 4 years' experience; IE-01—interobserver analysis by the first and second observer with 4 and 3 years' experience, respectively; IE-02—interobserver analysis by the first and third observer with 4 and 1 years' experience, respectively; IE-03—interobserver analysis by the second and third observer with 3 and 1 years' experience, respectively; WSS—wall shear stress; and LoA<sub>diff</sub>—relative difference in limits of agreement between the training and validation cohort.

## DISCUSSION

The main findings of the current study are: (1) hemodynamic parameters (i.e., normalized flow displacement, flow jet angle,  $\text{WSS}_{\text{mag}}$ ,  $\text{WSS}_{\text{ax}}$ ,  $\text{WSS}_{\text{cir}}$ ,  $\text{WSS}_{\text{angle}}$ , vorticity norm, absolute helicity, and volumes with increased absolute LNH) and morphological parameters (volume, centerline length, diameter and curvature radius) can be assessed with very good reproducibility in the thoracic aorta of TAA patients with a TAV, (2) the reproducibility of these parameters is slightly decreased within the aortic root, and (3) the reproducibility is affected by the observer's experience.

The intra- and interobserver analyses generally demonstrated a very good reproducibility for the assessment of hemodynamic parameters in TAA patients with a TAV. Similar results have been described previously for flow displacement, flow jet angle,  $\text{WSS}_{\text{mag}}$ ,  $\text{WSS}_{\text{angle}}$ , secondary flow patterns (which are reflected in vorticity and helicity), and volumes with increased absolute LNH in healthy volunteers and in patients with none-to-marginally dilated aortas (11-19, 30), but not yet in a clinically relevant patient group, such as patients with TAA. Moreover, the Bland–Altman plots of the current study demonstrated for most hemodynamic parameters and analyses no striking dependency of the measured differences relative to the mean.

Furthermore, the intra- and interobserver analyses demonstrated very good reproducibility of the morphologic parameters in TAA patients with a TAV. Similar reproducibility results have been described previously for volume, centerline length, maximal diameter, and curvature radius in healthy volunteers (25). However, the current study demonstrated wider LoAs for all morphologic parameters within TAA patients compared to healthy volunteers. These wider LoAs in TAA patients may potentially be associated with the presence of dilation since, for a constant flow rate, the blood velocity is inversely related to the vessel's diameter. Therefore, a larger area of reduced velocity-to-noise ratio is expected for TAA patients compared to healthy volunteers, especially close to the vessel wall. This reduced velocity-to-noise ratio potentially can have a negative influence on the reproducibility of aortic lumen segmentation. However, the velocity-to-noise ratio within these areas may be improved by 4D flow MRI sequences with multiple-velocity-encoding gradients, which consequently may also improve the reproducibility of hemodynamics parameters (31, 32).

When analyzing the results per anatomical segment, it was observed that the reproducibility was slightly reduced but still acceptable for most hemodynamic and morphologic parameters within the aortic root. This slight reduction in reproducibility was also seen in the proximal and distal ascending aorta for the maximal diameter. This reduced reproducibility is potentially introduced by the movement of the aortic root and ascending aorta in contrast to the relatively fixed-positioned aortic arch and descending aorta (33-35). This effect related to the cardiac movement (contraction and

relaxation) may further be amplified by the heart rate variation and breathing variation during the acquisition. Alongside, inadequate respiratory compensation or inadequate electrocardiographic gating may also perturbate the 4D flow MRI data. Moreover, within the aortic root, complex secondary flow patterns (recirculating flow) are present (9, 36). Since this recirculating flow has a relatively low velocity compared to the velocity-encoding sensitivity, these recirculating areas have a reduced velocity-to-noise ratio close to the vessel wall and potentially introduce more observer-dependent variability on the aortic lumen segmentation.

The observer-dependent variability of the 3D lumen segmentation was assessed directly by evaluating the variability in morphologic parameters. This analysis also demonstrated, for example, wider LoAs for the maximal diameter within the proximal part of the aorta (i.e., aortic root, proximal and distal ascending aorta) compared to thoracic aorta distal to the ascending part (intraobserver LoA  $\leq 2.7$  and  $\leq 1.8$  mm; interobserver LoA  $\leq 7.6$  and  $\leq 3.3$  mm, respectively). In contrast, a recent study assessing the interobserver reproducibility of manually measured diameters imaged with computed tomography demonstrated in the aortic root, ascending and descending aorta an LoA of 2.5, 2.1, and 1.9 mm, respectively (37). For MRI, it is recommended to measure the maximal diameter on an MRI sequence with an isotropic voxel size  $\leq 1.5$  mm to achieve a clinically acceptable accuracy (38). Since the 4D flow MRI sequence applied in the current study had an isotropic spatial resolution of 2.5–3.0 mm, the morphologic parameters derived from this sequence should not be used to define the maximal aortic diameter of TAA patients. However, for the quantification of hemodynamic parameters, an isotropic resolution of  $\leq 3.0$  mm is indicated as sufficient for the 4D flow MRI (23). Of note, the 4D flow MRI was acquired to assess the patient's aorta hemodynamics and therefore was not meant to describe the patient's aorta morphology (i.e., TAA diameter).

The decreased LoA within the validation cohort compared to the training cohort indicate that the reproducibility likely is affected by the observer's experience, especially for the aortic root, proximal, and distal ascending aorta. Moreover, the observer's experience likely plays a larger role in the assessment of morphologic parameters compared to the hemodynamic parameters, considering the decrease in LoA between the training and validation cohort. This result demonstrates the robustness of the image analysis for the quantification of hemodynamic parameters, despite the observer-dependent variability and experience.

No major limitations were observed for the hemodynamics quantification in the segments of the thoracic aorta. Although no clear reproducibility limitations were observed for TAA patients with a TAV, still some variation is present in the hemodynamic parameters. This variation must be taken into account when these hemodynamic parameters are used for the prediction of progressive dilation and adverse aortic events in TAA patients with a TAV.

A limitation of the present study was the small population size. However, the robustness of the study was improved by including multiple observers, analyzing five systolic phases, and dividing the thoracic aorta into six anatomical segments. This resulted in a total of 2400 lumen segments for which the hemodynamic and morphologic parameters were quantified. Moreover, future research should include patients with other aortic pathologies. Finally, for patients with TAA, no data were available on repeated 4D flow MRI acquisition; thus, interexamination reproducibility could not be assessed.

## **CONCLUSION**

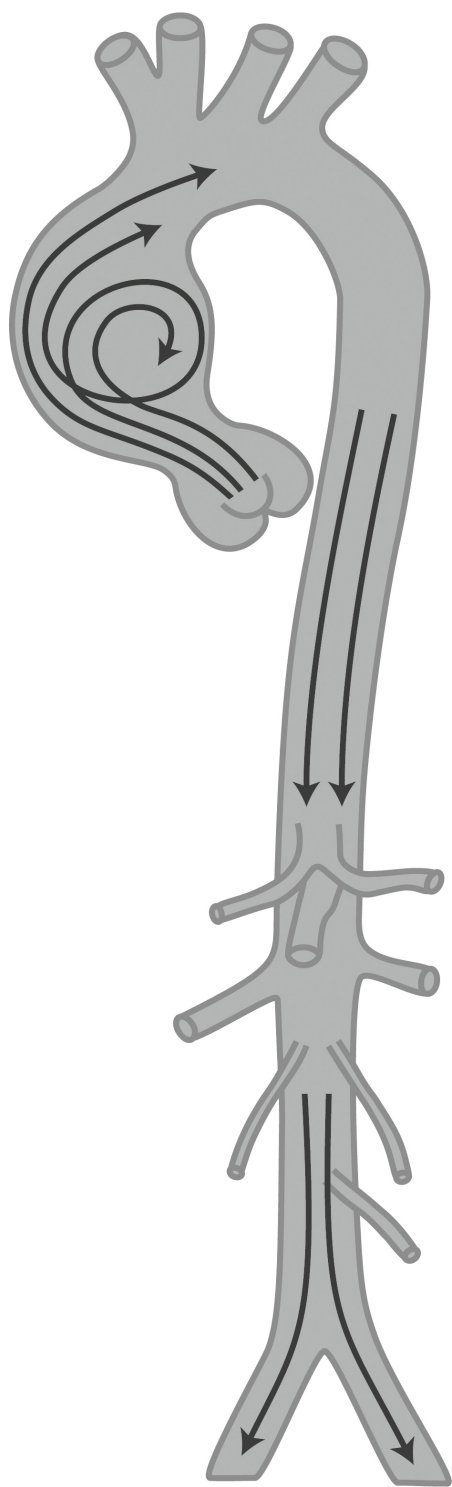
The current study demonstrated a very good reproducibility for all hemodynamic parameters within the thoracic aorta in TAA patients. This allows precise quantification of the patient's aorta hemodynamics from a 4D flow MRI.

## REFERENCES

1. Davies RR, Gallo A, Coady MA, Tellides G, Botta DM, Burke B, et al. Novel measurement of relative aortic size predicts rupture of thoracic aortic aneurysms. *The Annals of thoracic surgery*. 2006;81(1):169-77.
2. Hiratzka LF, Bakris GL, Beckman JA, Bersin RM, Carr VF, Casey DE, et al. 2010 ACCF/AHA/AATS/ACR/ASA/SCA/SCAI/SIR/STS/SVM guidelines for the diagnosis and management of patients with thoracic aortic disease. *Journal of the American College of Cardiology*. 2010;55(14):e27-e129.
3. Erbel R, Aboyans V, Boileau C, Bossone E, Bartolomeo RD, Eggebrecht H, et al. 2014 ESC Guidelines on the diagnosis and treatment of aortic diseases: Document covering acute and chronic aortic diseases of the thoracic and abdominal aorta of the adult The Task Force for the Diagnosis and Treatment of Aortic Diseases of the European Society of Cardiology (ESC). *European heart journal*. 2014;35(41):2873-926.
4. Pape LA, Tsai TT, Isselbacher EM, Oh JK, O'Gara PT, Evangelista A, et al. Aortic diameter $\geq$  5.5 cm is not a good predictor of type A aortic dissection: observations from the International Registry of Acute Aortic Dissection (IRAD). *Circulation*. 2007;116(10):1120-7.
5. Heuts S, Adriaans BP, Rylski B, Mihl C, Bekkers SC, Olsthoorn JR, et al. Evaluating the diagnostic accuracy of maximal aortic diameter, length and volume for prediction of aortic dissection. *Heart*. 2020;106(12):892-7.
6. Glower DD. Indications for Ascending Aortic Replacement: Size Alone Is Not Enough. *Journal of the American College of Cardiology*; 2011. p. 585-6.
7. van Hout M, Juffermans J, Lamb H, Kröner E, van den Boogaard P, Schalij M, et al. Ascending aorta curvature and flow displacement are associated with accelerated aortic growth at long-term follow-up: A MRI study in Marfan and thoracic aortic aneurysm patients. *IJC Heart & Vasculature*. 2022;38:100926.
8. Korpela T, Kauhanen SP, Kariniemi E, Saari P, Liimatainen T, Jaakkola P, et al. Flow displacement and decreased wall shear stress might be associated with the growth rate of an ascending aortic dilatation. *European Journal of Cardio-Thoracic Surgery*. 2022;61(2):395-402.
9. Ramaekers MJ, Adriaans BP, Juffermans JF, Van Assen HC, Bekkers SC, Scholte AJ, et al. Characterization of ascending aortic flow in patients with degenerative aneurysms: a 4D flow magnetic resonance study. *Investigative Radiology*. 2021;56(8):494-500.
10. Kauhanen SP, Hedman M, Kariniemi E, Jaakkola P, Vanninen R, Saari P, et al. Aortic dilatation associates with flow displacement and increased circumferential wall shear stress in patients without aortic stenosis: a prospective clinical study. *Journal of Magnetic Resonance Imaging*. 2019;50(1):136-45.
11. Dux-Santoy L, Guala A, Teixido-Tura G, Ruiz-Munoz A, Maldonado G, Villalva N, et al. Increased rotational flow in the proximal aortic arch is associated with its dilation in bicuspid aortic valve disease. *European Heart Journal-Cardiovascular Imaging*. 2019;20(12):1407-17.
12. Bissell MM, Hess AT, Biasioli L, Glaze SJ, Loudon M, Pitcher A, et al. Aortic dilation in bicuspid aortic valve disease: flow pattern is a major contributor and differs with valve fusion type. *Circulation: Cardiovascular Imaging*. 2013;6(4):499-507.
13. Garcia J, Barker AJ, Collins JD, Carr JC, Markl M. Volumetric quantification of absolute local normalized helicity in patients with bicuspid aortic valve and aortic dilatation. *Magnetic resonance in medicine*. 2017;78(2):689-701.
14. Lorenz R, Bock J, Barker A, von Knobelsdorff-Brenkenhoff F, Wallis W, Korvink J, et al. 4D flow magnetic resonance imaging in bicuspid aortic valve disease demonstrates altered distribution of aortic blood flow helicity. *Magnetic resonance in medicine*. 2014;71(4):1542-53.

15. Sigovan M, Hope MD, Dyverfeldt P, Saloner D. Comparison of four-dimensional flow parameters for quantification of flow eccentricity in the ascending aorta. *Journal of Magnetic Resonance Imaging*. 2011;34(5):1226-30.
16. Hope MD, Sigovan M, Wrenn SJ, Saloner D, Dyverfeldt P. MRI hemodynamic markers of progressive bicuspid aortic valve-related aortic disease. *Journal of Magnetic Resonance Imaging*. 2014;40(1):140-5.
17. den Reijer PM, Sallee D, van der Velden P, Zaaijer ER, Parks WJ, Ramamurthy S, et al. Hemodynamic predictors of aortic dilatation in bicuspid aortic valve by velocity-encoded cardiovascular magnetic resonance. *Journal of Cardiovascular Magnetic Resonance*. 2010;12(1):1-13.
18. Geiger J, Hirtler D, Gottfried K, Rahman O, Bollache E, Barker AJ, et al. Longitudinal evaluation of aortic hemodynamics in Marfan syndrome: new insights from a 4D flow cardiovascular magnetic resonance multi-year follow-up study. *Journal of Cardiovascular Magnetic Resonance*. 2017;19(1):1-11.
19. Minderhoud S, Roos-Hesselink J, Chelu R, Bons L, Van Den Hoven A, Korteland S, et al. Wall shear stress angle determines aortic growth in patients with bicuspid aortic valves. *European Heart Journal-Cardiovascular Imaging*. 2021;22(Supplement\_2):jeab090. 120.
20. van der Palen RLF, Roest AAW, van den Boogaard PJ, de Roos A, Blom NA, Westenberg JJM. Scan-rescan reproducibility of segmental aortic wall shear stress as assessed by phase-specific segmentation with 4D flow MRI in healthy volunteers. *MAGMA*. 2018 May 26. PubMed PMID: 29804208. Epub 2018/05/29.
21. Markl M, Wallis W, Harloff A. Reproducibility of flow and wall shear stress analysis using flow-sensitive four-dimensional MRI. *Journal of Magnetic Resonance Imaging*. 2011;33(4):988-94.
22. Van Ooij P, Powell AL, Potters WV, Carr JC, Markl M, Barker, et al. Reproducibility and interobserver variability of systolic blood flow velocity and 3D wall shear stress derived from 4D flow MRI in the healthy aorta. *Journal of Magnetic Resonance Imaging*. 2016;43(1):236-48.
23. Dyverfeldt P, Bissell M, Barker AJ, Bolger AF, Carlhäll C-J, Ebbers T, et al. 4D flow cardiovascular magnetic resonance consensus statement. *Journal of Cardiovascular Magnetic Resonance*. 2015;17(1):72.
24. Petersson S, Dyverfeldt P, Ebbers T. Assessment of the accuracy of MRI wall shear stress estimation using numerical simulations. *Journal of Magnetic Resonance Imaging*. 2012;36(1):128-38.
25. Juffermans JF, Westenberg JJ, van den Boogaard PJ, Roest AA, van Assen HC, van der Palen RL, et al. Reproducibility of aorta segmentation on 4D flow MRI in healthy volunteers. *Journal of Magnetic Resonance Imaging*. 2020.
26. Wentland AL. Editorial for "Reproducibility of Aorta Segmentation on 4D Flow MRI in Healthy Volunteers". Wiley Online Library; 2021.
27. Della Corte A, Bancone C, Dialetto G, Covino FE, Manduca S, Montibello MV, et al. The ascending aorta with bicuspid aortic valve: a phenotypic classification with potential prognostic significance. *European Journal of Cardio-Thoracic Surgery*. 2014;46(2):240-7.
28. Virtanen P, Gommers R, Oliphant TE, Haberland M, Reddy T, Cournapeau D, et al. SciPy 1.0: fundamental algorithms for scientific computing in Python. *Nature methods*. 2020;17(3):261-72.
29. Bland JM, Altman DG. Statistical methods for assessing agreement between two methods of clinical measurement. *lancet*. 1986;1(8476):307-10.
30. Meierhofer C, Schneider EP, Lyko C, Hutter A, Martinoff S, Markl M, et al. Wall shear stress and flow patterns in the ascending aorta in patients with bicuspid aortic valves differ significantly from tricuspid aortic valves: a prospective study. *European Heart Journal-Cardiovascular Imaging*. 2013;14(8):797-804.

31. Schnell S, Rose MJ, Wu C, Garcia J, Robinson JD, Markl M, et al. Improved assessment of aortic hemodynamics by kt accelerated dual-VENC 4D flow MRI in pediatric patients. *Journal of Cardiovascular Magnetic Resonance*. 2016;18(1):1-2.
32. Ma LE, Markl M, Chow K, Vali A, Wu C, Schnell S. Efficient triple-VENC phase-contrast MRI for improved velocity dynamic range. *Magnetic Resonance in Medicine*. 2019.
33. Bons LR, Duijnhouwer AL, Boccalini S, Van Den Hoven AT, Van Der Vlugt MJ, Chelu RG, et al. Intermodality variation of aortic dimensions: How, where and when to measure the ascending aorta. *International journal of cardiology*. 2019;276:230-5.
34. Bell V, Mitchell WA, Sigurðsson S, Westenberg JJ, Gotal JD, Torjesen AA, et al. Longitudinal and circumferential strain of the proximal aorta. *Journal of the American Heart Association*. 2014;3(6):e001536.
35. Rengier F, Weber TF, Henninger V, Böckler D, Schumacher H, Kauczor H-U, et al. Heartbeat-related distension and displacement of the thoracic aorta in healthy volunteers. *European journal of radiology*. 2012;81(1):158-64.
36. Kilner PJ, Yang GZ, Mohiaddin RH, Firmin DN, Longmore DB. Helical and retrograde secondary flow patterns in the aortic arch studied by three-directional magnetic resonance velocity mapping. *Circulation*. 1993;88(5):2235-47.
37. Dux-Santoy L, Rodríguez-Palomares JF, Teixidó-Turà G, Ruiz-Muñoz A, Casas G, Valente F, et al. Registration-based semi-automatic assessment of aortic diameter growth rate from contrast-enhanced computed tomography outperforms manual quantification. *European Radiology*. 2022;32(3):1997-2009.
38. van Hout MJ, Scholte AJ, Juffermans JF, Westenberg JJ, Zhong L, Zhou X, et al. How to Measure the Aorta Using MRI: A Practical Guide. *Journal of magnetic resonance imaging: JMRI*. 2020:e27183.



# Supplemental Tables to Chapter 3

---

**Supplemental Table S1.** Characteristics of the 4D flow MRI sequence.

MRI scanner	Ingenia [n=8] and Elition [n=12], Philips Healthcare, Best, The Netherlands
Respiratory motion compensation	Hemidiaphragm respiratory navigator
Electrocardiographic gating	Retrospective
Field of view [mm <sup>3</sup> ]	350 x 260–360 x 62–106
Acquired isotropic spatial resolution [mm <sup>3</sup> ]	2.5 – 3.0
Temporal resolution [ms]	27 – 34
Echo time [ms]	2.5 – 2.9
Repetition time [ms]	4.4 – 4.8
Flip angle [°]	10
Planned acquisition time* [s]	504 ± 69
Segmentation factor (Turbo field echo factor)	2

Data notated as the mean ± standard deviation or with upper – lower limits. \*excluding hemidiaphragm respiratory navigator.

**Supplemental Table S2.** Intra- and Interobserver reproducibility: results of the training cohort.

Study	Bland-Altman			Spearman Rank Correlation Coefficient	Intraclass Correlation Coefficient
	Mean Diff	LoA	COV [%]		
Flow Displacement [%]					
IA-0	0.0	3.1	21	0.76	0.92
IE-01	-0.6	4.2	27	0.68	0.87
IE-02	-0.2	4.3	29	0.68	0.86
IE-03	0.4	3.8	25	0.74	0.90
Flow Jet Angle [°]					
IA-0	0.1	6.0	20	0.81	0.91
IE-01	0.2	8.4	27	0.78	0.84
IE-02	0.6	7.8	26	0.75	0.86
IE-03	0.5	9.1	30	0.73	0.81
WSS Magnitude [mPa]					
IA-0	10	80	5	0.99	0.99
IE-01	7	253	17	0.88	0.90
IE-02	45	202	14	0.92	0.93
IE-03	38	231	16	0.91	0.92
Axial WSS [mPa]					
IA-0	8	79	6	0.99	0.99
IE-01	6	249	18	0.90	0.91
IE-02	42	209	16	0.92	0.94
IE-03	36	230	17	0.91	0.93
Circumferential WSS [mPa]					
IA-0	4	43	9	0.98	0.97
IE-01	12	85	18	0.9	0.88
IE-02	22	88	19	0.9	0.88
IE-03	11	85	19	0.88	0.87
WSS Angle [°]					
IA-0	0.2	4.0	9	0.98	0.98
IE-01	-0.6	8.4	19	0.93	0.93
IE-02	-1.0	10.4	23	0.95	0.91
IE-03	-0.4	9.6	21	0.94	0.93
Vorticity Norm [ $s^{-1} \cdot mL^{-1}$ ]					
IA-0	83	1,007	4	0.99	1.00
IE-01	359	2,226	8	0.97	0.98
IE-02	704	3,319	12	0.96	0.95
IE-03	346	2,131	8	0.98	0.98

**Supplemental Table S2. Continued**

Study	Bland-Altman			Spearman Rank Correlation Coefficient	Intraclass Correlation Coefficient
	Mean Diff	LoA	COV [%]		
Absolute Helicity [ $\text{m}\cdot\text{s}^{-2}\cdot\text{mL}^{-1}$ ]					
IA-O	61	538	14	1.00	0.98
IE-01	83	936	25	0.99	0.94
IE-02	123	1,233	33	0.98	0.89
IE-03	39	417	12	0.99	0.99
Absolute Local Normalized Helicity Volume [mL]					
IA-O	0.4	3.0	9	0.98	0.98
IE-01	0.6	7.2	21	0.87	0.90
IE-02	0.6	8.4	24	0.85	0.87
IE-03	0.0	8.2	24	0.85	0.86
Volume [mL]					
IA-O	0.7	6.5	8	0.97	0.97
IE-01	1.5	16.0	21	0.79	0.82
IE-02	1.9	18.2	24	0.77	0.80
IE-03	0.4	18.1	24	0.78	0.78
Centerline Length [mm]					
IA-O	1.2	7.6	8	0.97	0.96
IE-01	2.5	18.7	21	0.73	0.77
IE-02	2.3	15.2	17	0.89	0.87
IE-03	-0.1	16.9	19	0.80	0.83
Maximal Diameter [mm]					
IA-O	0.1	2.2	3	0.99	0.99
IE-01	0.1	4.2	6	0.97	0.97
IE-02	-1.1	8.5	11	0.92	0.89
IE-03	-1.2	6.7	9	0.95	0.93
Curvature Radius [mm]					
IA-O	-0.4	28.7	21	0.87	0.96
IE-01	2.2	40.8	31	0.76	0.90
IE-02	-9.1	149.5	105	0.69	0.41
IE-03	-11.3	145.8	104	0.79	0.40

Characteristics are presented per cohort over all subjects, anatomical segments and systolic phases ( $n = 300$ ). \* – All probability values  $< 0.01$ . Abbreviations: Mean Diff – mean difference, LoA – limits of agreement ( $1.96 \times$  standard deviation), COV = coefficient of variation, IA-O – intraobserver, IE-O – interobserver, IE-E – interexamination, and WSS – wall shear stress

Supplemental Table S3. Intraobserver reproducibility: results of both cohorts per anatomical segment.

Cohort	Training cohort						Validation cohort						
	Bland-Altman			Spearman Rank Correlation Coefficient			Bland-Altman			Spearman Rank Correlation Coefficient			
	Seg	Mean Diff	LoA	COV [%]	r	p	Mean Diff	LoA	cov [%]	r	p		
Flow Displacement [‰]													
AoR	-0.8	4.1	28	0.72	<0.01		0.82	-0.6	2.8	16	0.94	<0.01	0.93
pAA	0.5	2.4	11	0.93	<0.01		0.98	0.3	2.4	10	0.98	<0.01	0.98
dAA	0.4	3.2	20	0.84	<0.01		0.93	-0.1	2.6	19	0.81	<0.01	0.95
AoA	0.2	2.6	23	0.59	<0.01		0.59	0.2	3.3	30	0.26	0.07	0.24
pDA	0.1	2.7	19	0.63	<0.01		0.78	0.0	3.2	25	0.37	0.01	0.52
dDA	-0.0	2.5	24	0.74	<0.01		0.64	-0.1	2.1	23	0.52	<0.01	0.56
Flow Jet Angle [°]													
AoR	-0.6	9.4	28	0.37	<0.01		0.72	0.7	7.2	18	0.78	<0.01	0.84
pAA	-0.0	4.9	13	0.92	<0.01		0.97	0.2	4.8	12	0.95	<0.01	0.95
dAA	0.3	5.8	19	0.84	<0.01		0.95	0.5	5.0	14	0.94	<0.01	0.95
AoA	1.1	4.8	16	0.81	<0.01		0.83	0.3	3.7	13	0.85	<0.01	0.84
pDA	0.1	5.4	17	0.85	<0.01		0.83	0.0	4.4	14	0.87	<0.01	0.87
dDA	-0.1	3.8	18	0.64	<0.01		0.83	-0.1	4.4	27	0.64	<0.01	0.62
WSS Magnitude [mPa]													
AoR	40	151	13	0.94	<0.01		0.90	-12	76	7	0.95	<0.01	0.94
pAA	-5	64	5	0.99	<0.01		0.99	-8	32	2	1.00	<0.01	1.00
dAA	5	34	2	0.99	<0.01		1.00	0	14	1	1.00	<0.01	1.00
AoA	2	58	4	0.99	<0.01		0.99	0	25	2	1.00	<0.01	1.00

### **Supplemental Table S3. Continued**

Supplemental Table S3. Continued

Cohort	Training cohort						Validation cohort					
	Bland-Altman			Spearman Rank Correlation Coefficient			Bland-Altman			Spearman Rank Correlation Coefficient		
	Seg	Mean Diff	LoA	Cov [%]	r	p	Correlation Coefficient	Mean Diff	LoA	Cov [%]	r	p
dAA	0.1	3.2	9	0.97	<0.01		0.98	0.1	2.2	6	0.98	<0.01
AoA	1.1	4.5	15	0.97	<0.01		0.92	-0.2	2.3	8	0.94	<0.01
pDA	-0.1	2.8	8	0.95	<0.01		0.94	-0.5	2.0	6	0.96	<0.01
dDA	-0.3	2.9	11	0.93	<0.01		0.92	-0.0	2.2	9	0.95	<0.01
Vorticity Norm [ $s^{-1} \cdot mL^{-1}$ ]												
AoR	142	1,171	3	0.98	<0.01		0.99	193	1,265	4	0.95	<0.01
pAA	258	1,524	6	0.98	<0.01		0.98	78	776	3	0.99	<0.01
dAA	127	725	4	0.99	<0.01		1.00	0	485	2	1.00	<0.01
AoA	-3	586	3	0.99	<0.01		1.00	22	685	3	1.00	<0.01
pDA	-97	800	3	0.99	<0.01		1.00	-133	508	2	1.00	<0.01
dDA	74	768	3	0.99	<0.01		1.00	64	1,024	3	0.99	<0.01
Absolute Helicity [ $m \cdot s^{-2} \cdot mL^{-1}$ ]												
AoR	242	1,163	16	0.99	<0.01		0.95	24	411	8	0.95	<0.01
pAA	86	414	11	0.99	<0.01		0.98	80	203	5	0.99	<0.01
dAA	19	87	4	1.00	<0.01		1.00	1	65	3	0.99	<0.01
AoA	-6	92	4	1.00	<0.01		1.00	3	70	2	1.00	<0.01
pDA	-5	74	2	1.00	<0.01		1.00	-1	85	2	1.00	<0.01
dDA	27	135	4	1.00	<0.01		1.00	70	214	5	1.00	<0.01

### Supplemental Table S3. Continued

Cohort	Training cohort						Validation cohort					
	Bland-Altman			Spearman Rank Correlation Coefficient			Intraclass Correlation Coefficient Mean Diff			Bland-Altman		
	Seg	Mean Diff	LoA	COV [%]	r	p	Absolute	Local	Normalized	Helicity	Volume [mL]	
Volume [mL]												
AoR	-0.3	4.8	14	0.95	<0.01		0.95		-1.2	6.5	15	0.91
pAA	-0.3	2.7	5	0.97	<0.01		0.98		2.7	6	0.99	<0.01
dAA	0.7	2.8	8	0.98	<0.01		0.99		0.4	1.0	3	1.00
AoA	0.9	1.7	8	0.98	<0.01		0.99		-0.2	1.4	7	0.98
pDA	0.6	2.3	8	0.95	<0.01		0.97		0.2	1.9	6	0.96
dDA	0.6	1.8	5	0.95	<0.01		0.98		0.3	1.5	5	0.96
Centerline Length [mm]												
AoR	-0.8	10.3	13	0.94	<0.01		0.94		-2.4	12.1	13	0.93
pAA	-0.6	5.8	6	0.91	<0.01		0.98		1.5	5.6	6	0.98
dAA	1.3	6.8	7	0.95	<0.01		0.97		1.0	3.0	4	0.98
AoA	1.9	3.9	7	0.94	<0.01		0.97		-0.4	2.9	6	0.96
pDA	1.4	4.9	7	0.96	<0.01		0.97		0.9	5.3	7	0.97
dDA	0.8	2.7	4	0.94	<0.01		0.99		0.5	3.9	7	0.95

Supplemental Table S3. Continued

Cohort	Training cohort						Validation cohort						
	Bland-Altman			Spearman Rank Correlation Coefficient			Bland-Altman			Spearman Rank Correlation Coefficient			
	Seg	Mean Diff	LoA	COV [%]	r	p	Correlation Coefficient	Mean Diff	LoA	COV [%]	r	p	Intraclass Correlation Coefficient
pDA	3.1	9.1	7	0.87	<0.01		0.80	2.5	7.9	6	0.97	<0.01	0.94
dDA	2.6	9.2	7	0.83	<0.01		0.80	2.3	8.1	7	0.98	<0.01	0.93
Maximal Diameter [mm]													
AoR	-0.3	2.2	2	0.94	<0.01		0.99	-0.4	2.7	3	0.85	<0.01	0.98
pAA	0.0	3.0	3	0.88	<0.01		0.93	0.1	2.5	3	0.91	<0.01	0.94
dAA	0.2	1.7	2	0.96	<0.01		0.99	0.1	1.1	1	0.99	<0.01	0.99
AoA	0.5	2.4	3	0.97	<0.01		0.95	-0.4	1.8	3	0.96	<0.01	0.97
pDA	0.1	1.5	2	0.89	<0.01		0.97	-0.4	0.9	2	0.97	<0.01	0.99
dDA	-0.2	1.4	3	0.95	<0.01		0.97	-0.2	1.1	2	0.94	<0.01	0.98
Curvature Radius [mm]													
AoR	2.0	43.5	35	0.38	0.01		0.46	4.8	66.7	61	0.46	<0.01	0.42
pAA	1.2	8.9	11	0.74	<0.01		0.82	-0.5	8.0	10	0.91	<0.01	0.82
dAA	-2.2	17.5	15	0.85	<0.01		0.89	-0.2	7.2	7	0.92	<0.01	0.93
AoA	1.0	12.7	14	0.81	<0.01		0.82	5.8	42.4	37	0.87	<0.01	0.56
pDA	1.7	6.3	7	0.92	<0.01		0.93	1.2	3.8	5	0.83	<0.01	0.96
dDA	-6.0	47.6	16	0.91	<0.01		0.95	2.4	42.2	15	0.91	<0.01	0.94

Characteristics are presented per anatomical segment over all subjects, systolic phases ( $n = 60$ ). Abbreviations: Seg – anatomical segment, Mean Diff – mean difference, LoA – limits of agreement ( $1.96 \times$  standard deviation difference), COV – coefficient of variation, ICC – intraclass correlation coefficient, WSS – wall shear stress, AoR – aortic root, pAA – proximal ascending aorta, dAA – distal ascending aorta, AoA – aortic arch, pDA – proximal descending aorta, and dDA – distal descending aorta.

**Supplemental Table S4.** Interobserver reproducibility: results of both cohorts per anatomical segment.

Seg	Cohort	Training cohort						Validation cohort					
		Bland-Altman			Spearman Rank Correlation Coefficient			Bland-Altman			Spearman Rank Correlation Coefficient		
		Analysis	Mean Diff	LoA	Cov [%]	r	p	Intraclass Correlation Coefficient	Mean Diff	LoA	Cov [%]	r	p
Flow Displacement [%]													
AoR	1	-1.6	6.4	41	0.62	<0.01	0.61	-0.9	8.9	49	0.16	0.27	0.19
	2	-0.8	6.0	41	0.58	<0.01	0.59	-0.3	7.0	40	0.43	<0.01	0.48
	3	0.8	4.3	26	0.76	<0.01	0.84	0.6	4.3	23	0.74	<0.01	0.77
pAA	1	-0.3	3.6	16	0.81	<0.01	0.95	-0.5	3.9	16	0.94	<0.01	0.94
	2	-0.2	3.6	16	0.88	<0.01	0.96	0.7	4.8	21	0.92	<0.01	0.91
	3	0.1	3.7	17	0.86	<0.01	0.96	1.2	5.2	21	0.90	<0.01	0.89
dAA	1	-0.3	3.2	19	0.80	<0.01	0.93	-0.6	3.5	25	0.61	<0.01	0.92
	2	0.1	3.6	22	0.84	<0.01	0.92	-0.1	4.3	31	0.77	<0.01	0.86
	3	0.4	3.1	18	0.78	<0.01	0.94	0.4	5.0	35	0.63	<0.01	0.80
AoA	1	-0.8	3.7	31	0.39	<0.01	0.34	-0.9	3.4	29	0.53	<0.01	0.39
	2	-0.0	2.4	21	0.76	<0.01	0.69	0.2	2.6	24	0.45	<0.01	0.49
	3	0.8	3.1	26	0.53	<0.01	0.52	1.1	3.1	26	0.59	<0.01	0.52
pDA	1	-0.5	3.6	24	0.45	<0.01	0.63	-0.2	3.0	23	0.47	<0.01	0.56
	2	-0.0	3.3	23	0.56	<0.01	0.72	0.2	3.5	28	0.33	0.02	0.41
	3	0.5	3.3	22	0.66	<0.01	0.74	0.4	3.4	27	0.46	<0.01	0.53
dDA	1	0.2	2.5	24	0.66	<0.01	0.61	0.2	2.5	28	0.43	<0.01	0.42
	2	-0.2	5.4	51	0.44	<0.01	0.07	-0.1	2.3	26	0.43	<0.01	0.47
	3	-0.4	4.5	43	0.67	<0.01	0.34	-0.2	1.7	19	0.75	<0.01	0.71

Supplemental Table S4. Continued

Seg	Analysis	Training cohort						Validation cohort					
		Bland-Altman			Spearman Rank Correlation Coefficient			Bland-Altman			Spearman Rank Correlation Coefficient		
		Mean Diff	LoA	Cov [%]	r	p	Mean Diff	LoA	Cov [%]	r	p		
Flow Jet Angle [°]													
AoR	1	-0.7	13.9	42	0.21	0.15	0.27	0.2	12.1	30	0.47	<0.01	0.54
	2	3.0	12.9	44	0.34	0.02	0.50	-0.1	7.9	19	0.77	<0.01	0.77
	3	3.7	16.4	54	0.22	0.12	0.18	-0.3	10.9	27	0.49	<0.01	0.52
pAA	1	0.1	6.1	16	0.93	<0.01	0.95	-0.9	9.4	24	0.78	<0.01	0.76
	2	-1.2	6.5	17	0.88	<0.01	0.94	0.4	7.2	19	0.87	<0.01	0.87
	3	-1.4	6.0	16	0.91	<0.01	0.95	1.3	10.9	28	0.69	<0.01	0.68
dAA	1	-1.1	8.1	25	0.83	<0.01	0.92	0.7	8.6	25	0.76	<0.01	0.87
	2	-0.4	6.3	20	0.84	<0.01	0.95	1.3	8.3	25	0.85	<0.01	0.87
	3	0.7	5.9	18	0.91	<0.01	0.96	0.6	8.9	27	0.83	<0.01	0.87
AoA	1	-0.1	6.7	22	0.67	<0.01	0.67	0.4	4.3	16	0.66	<0.01	0.71
	2	1.0	5.9	20	0.70	<0.01	0.70	0.2	5.7	20	0.72	<0.01	0.67
	3	1.1	6.5	22	0.56	<0.01	0.61	-0.2	6.9	25	0.44	<0.01	0.46
pDA	1	2.0	6.5	21	0.71	<0.01	0.75	-1.8	5.4	17	0.69	<0.01	0.77
	2	0.6	5.6	18	0.81	<0.01	0.83	-0.1	7.0	23	0.49	<0.01	0.49
	3	-1.5	5.2	17	0.72	<0.01	0.80	1.7	6.6	20	0.58	<0.01	0.58
dDA	1	0.6	3.3	16	0.67	<0.01	0.89	-0.5	3.2	19	0.73	<0.01	0.77
	2	0.8	3.1	15	0.79	<0.01	0.90	-0.4	5.2	31	0.71	<0.01	0.57
	3	0.1	3.7	19	0.61	<0.01	0.87	0.1	5.4	31	0.78	<0.01	0.55

Supplemental Table S4. Continued

Seg	Cohort	Training cohort						Validation cohort					
		Bland-Altman			Spearman Rank Correlation Coefficient			Bland-Altman			Spearman Rank Correlation Coefficient		
		Analysis	Mean Diff	LoA	Cov [%]	r	p	Mean Diff	Mean	Diff	LoA	Cov [%]	r
WSS Magnitude [mPa]													
AoR	1	97	288	25	0.67	<0.01	0.54	1	225	21	0.44	<0.01	0.39
	2	183	328	31	0.44	<0.01	0.38	-6	195	18	0.63	<0.01	0.63
	3	86	163	17	0.55	<0.01	0.65	-7	220	20	0.52	<0.01	0.52
pAA	1	28	233	17	0.87	<0.01	0.88	12	234	16	0.79	<0.01	0.78
	2	74	124	9	0.96	<0.01	0.96	51	160	11	0.95	<0.01	0.92
	3	46	282	22	0.82	<0.01	0.79	39	278	19	0.80	<0.01	0.71
dAA	1	-1	196	13	0.91	<0.01	0.95	-11	180	12	0.90	<0.01	0.93
	2	17	70	5	0.99	<0.01	0.99	6	112	7	0.95	<0.01	0.98
	3	18	205	14	0.92	<0.01	0.94	17	183	12	0.92	<0.01	0.93
	1	-46	192	13	0.91	<0.01	0.93	-60	184	11	0.92	<0.01	0.92
AoA	2	-14	68	5	0.99	<0.01	0.99	-5	143	9	0.94	<0.01	0.96
	3	32	203	14	0.92	<0.01	0.92	55	179	11	0.92	<0.01	0.92
	1	-20	238	14	0.85	<0.01	0.90	-76	217	11	0.91	<0.01	0.95
pDA	2	-3	44	3	0.99	<0.01	1.00	17	136	7	0.96	<0.01	0.98
	3	17	238	14	0.83	<0.01	0.90	92	223	11	0.92	<0.01	0.94
	1	-19	257	14	0.84	<0.01	0.91	-67	274	12	0.89	<0.01	0.93
dDA	2	10	66	4	0.98	<0.01	0.99	38	170	8	0.96	<0.01	0.97
	3	29	-	13	0.82	<0.01	0.91	105	270	12	0.90	<0.01	0.94

Supplemental Table S4. Continued

Seg	Analysis	Training cohort						Validation cohort					
		Bland-Altman			Spearman Rank Correlation Coefficient			Intraclass Correlation Coefficient			Bland Altman		
		Mean Diff	Cov [%]	r	p	Mean Diff	Mean Diff	Mean Diff	Mean	LoA	Cov [%]	r	p
Axial WSS [mPa]													
AoR	1	84	279	33	0.58	<0.01	0.45	0	187	25	0.40	<0.01	0.36
	2	179	324	43	0.27	0.05	0.18	-4	174	23	0.39	<0.01	0.48
	3	95	152	23	0.54	<0.01	0.50	-4	195	26	0.42	<0.01	0.36
pAA	1	37	228	20	0.87	<0.01	0.87	44	228	20	0.73	<0.01	0.71
	2	91	154	14	0.92	<0.01	0.92	61	160	14	0.94	<0.01	0.9
	3	54	285	27	0.78	<0.01	0.76	18	272	25	0.77	<0.01	0.63
dAA	1	6	193	14	0.92	<0.01	0.95	-8	196	14	0.90	<0.01	0.92
	2	14	68	5	0.99	<0.01	0.99	12	120	9	0.95	<0.01	0.97
	3	7	199	15	0.93	<0.01	0.95	20	197	14	0.94	<0.01	0.92
AoA	1	-45	193	14	0.92	<0.01	0.93	-62	197	13	0.91	<0.01	0.91
	2	-18	68	5	0.99	<0.01	0.99	-3	146	10	0.95	<0.01	0.95
	3	27	199	14	0.92	<0.01	0.93	59	190	12	0.91	<0.01	0.92
pDA	1	-25	240	15	0.85	<0.01	0.90	-79	223	12	0.91	<0.01	0.94
	2	-13	52	3	0.99	<0.01	0.99	15	147	8	0.96	<0.01	0.97
	3	12	231	14	0.84	<0.01	0.91	94	224	12	0.92	<0.01	0.94
dDA	1	-19	260	15	0.84	<0.01	0.90	-73	291	14	0.87	<0.01	0.93
	2	1	73	4	0.98	<0.01	0.99	34	184	9	0.96	<0.01	0.97
	3	20	245	14	0.84	<0.01	0.91	107	284	13	0.88	<0.01	0.93

Supplemental Table S4. Continued

Seg	Cohort	Training cohort						Validation cohort						
		Bland-Altman			Spearman Rank Correlation Coefficient			Bland-Altman			Spearman Rank Correlation Coefficient			
		Analysis	Mean Diff	LoA	Cov [%]	r	p	Intraclass Correlation Coefficient	Mean Diff	LoA	Cov [%]	r	p	
Circumferential WSS [mPa]														
AoR	1	50	99	16	0.80	<0.01	0.74	0.52	-5	101	15	0.62	<0.01	0.63
	2	55	145	24	0.47	<0.01						0.85	<0.01	0.82
	3	5	91	16	0.61	<0.01	0.74	-17	127	19	0.69	<0.01	0.69	
pAA	1	-3	124	21	0.76	<0.01	0.81	-31	131	18	0.63	<0.01	0.68	
	2	-3	82	14	0.88	<0.01	0.93	-2	105	15	0.81	<0.01	0.84	
	3	0	132	22	0.68	<0.01	0.76	29	132	18	0.72	<0.01	0.71	
dAA	1	-7	60	14	0.94	<0.01	0.94	-6	79	18	0.74	<0.01	0.72	
	2	16	60	15	0.96	<0.01	0.93	-10	58	13	0.84	<0.01	0.88	
	3	24	69	17	0.94	<0.01	0.91	-4	94	21	0.63	<0.01	0.63	
AoA	1	9	33	9	0.94	<0.01	0.95	3	52	14	0.77	<0.01	0.76	
	2	10	35	10	0.90	<0.01	0.94	-2	35	9	0.90	<0.01	0.9	
	3	1	43	12	0.91	<0.01	0.91	-5	61	16	0.66	<0.01	0.64	
pDA	1	17	59	13	0.83	<0.01	0.87	4	54	11	0.83	<0.01	0.92	
	2	24	54	12	0.90	<0.01	0.90	8	35	7	0.94	<0.01	0.97	
	3	7	67	16	0.83	<0.01	0.84	3	51	11	0.88	<0.01	0.93	
dDA	1	4	42	11	0.91	<0.01	0.91	18	76	20	0.73	<0.01	0.73	
	2	31	58	17	0.77	<0.01	0.79	30	59	16	0.85	<0.01	0.84	
	3	26	63	19	0.69	<0.01	0.73	11	100	29	0.73	<0.01	0.54	

Supplemental Table S4. Continued

Seg	Analysis	Training cohort						Validation cohort					
		Bland-Altman			Spearman Rank Correlation Coefficient			Bland Altman			Spearman Rank Correlation Coefficient		
		Mean Diff	Cov [%]	r	p	Mean Diff	Correlation Coefficient	Mean	Diff	LoA	Cov [%]	r	p
WSS Angle [°]													
AoR	1	-0.9	9.4	12	0.30	0.03	0.19	0.0	8.3	9	0.63	<0.01	0.62
	2	-6.4	12.7	15	0.05	0.70	0.07	-0.1	8.9	10	0.51	<0.01	0.61
	3	-5.5	8.9	11	0.50	<0.01	0.43	-0.1	10.3	12	0.48	<0.01	0.46
pAA	1	-3.0	11.0	18	0.75	<0.01	0.77	-3.8	9.5	14	0.55	<0.01	0.58
	2	-5.1	11.1	17	0.79	<0.01	0.78	-3.3	8.3	12	0.73	<0.01	0.8
	3	-2.2	13.7	20	0.67	<0.01	0.61	0.4	10.0	14	0.71	<0.01	0.6
dAA	1	-2.2	6.4	16	0.95	<0.01	0.93	-0.3	10.0	25	0.65	<0.01	0.65
	2	0.2	5.1	14	0.96	<0.01	0.95	-1.7	8.5	21	0.87	<0.01	0.84
	3	2.4	5.4	14	0.95	<0.01	0.96	-1.4	10.3	25	0.72	<0.01	0.69
AoA	1	1.2	4.8	16	0.77	<0.01	0.93	1.5	6.1	23	0.43	<0.01	0.43
	2	1.5	3.3	11	0.93	<0.01	0.96	-0.3	3.9	13	0.85	<0.01	0.84
	3	0.2	3.2	11	0.76	<0.01	0.97	-1.8	6.1	22	0.49	<0.01	0.51
pDA	1	1.0	7.1	21	0.80	<0.01	0.71	1.8	6.1	20	0.57	<0.01	0.52
	2	2.0	4.9	15	0.87	<0.01	0.84	0.1	4.9	15	0.77	<0.01	0.77
	3	1.0	6.0	19	0.87	<0.01	0.81	-1.6	5.1	17	0.70	<0.01	0.66
dDA	1	0.1	6.3	24	0.81	<0.01	0.72	1.6	7.2	33	0.41	<0.01	0.39
	2	2.0	4.6	19	0.87	<0.01	0.81	0.9	5.7	25	0.85	<0.01	0.78
	3	1.8	6.1	26	0.75	<0.01	0.72	-0.7	7.7	37	0.58	<0.01	0.47

Supplemental Table S4. Continued

Seg	Cohort	Training cohort						Validation cohort												
		Bland-Altman			Spearman Rank Correlation Coefficient			Intraclass Correlation Coefficient			Bland-Altman			Spearman Rank Correlation Coefficient						
		Analysis	Mean Diff	LoA	Cov [%]	r	p	Mean Diff	Mean	Diff	LoA	Cov [%]	r	p	Mean Diff	Mean	Diff	LoA	Cov [%]	r
Vorticity Norm [ $\text{s}^{-1} \cdot \text{mL}^{-1}$ ]																				
AoR	1	988	3,080	8	0.92	<0.01	0.95	462	1,738	5	0.91	<0.01	0.93							
	2	1,945	5,241	13	0.82	<0.01	0.84	-559	3,459	10	0.74	<0.01	0.72							
	3	957	3,017	8	0.93	<0.01	0.94	-1,021	3,700	10	0.66	<0.01	0.67							
	1	-285	3,004	12	0.91	<0.01	0.94	-1,198	2,324	8	0.92	<0.01	0.91							
pAA	2	-813	3,721	14	0.92	<0.01	0.90	-269	2,515	9	0.91	<0.01	0.90							
	3	-528	2,847	11	0.93	<0.01	0.94	929	2,262	8	0.93	<0.01	0.92							
	1	305	1,284	6	0.95	<0.01	0.99	198	1,103	6	0.99	<0.01	0.99							
dAA	2	788	1,594	8	0.96	<0.01	0.98	-104	1,514	7	0.97	<0.01	0.97							
	3	483	1,133	6	0.98	<0.01	0.99	-302	1,547	8	0.97	<0.01	0.97							
	1	401	1,027	5	0.99	<0.01	0.99	485	1,043	4	0.99	<0.01	0.99							
AoA	2	614	1,380	7	0.97	<0.01	0.97	452	1,872	8	0.96	<0.01	0.97							
	3	213	1,110	5	0.98	<0.01	0.98	-34	2,172	9	0.97	<0.01	0.95							
	1	88	903	3	0.99	<0.01	0.99	331	1,316	4	1.00	<0.01	0.99							
pDA	2	589	1,360	5	0.97	<0.01	0.99	83	1,904	6	0.98	<0.01	0.99							
	3	502	847	3	0.99	<0.01	0.99	-248	2,621	8	0.97	<0.01	0.97							
	1	655	1,991	8	0.99	<0.01	0.98	800	1,431	5	0.99	<0.01	0.99							
dDA	2	1,103	1,736	7	0.99	<0.01	0.98	956	1,927	6	0.97	<0.01	0.99							
	3	448	1,467	6	0.98	<0.01	0.99	156	2,389	8	0.97	<0.01	0.98							

Supplemental Table S4. Continued

Seg	Analysis	Training cohort						Validation cohort					
		Bland-Altman			Spearman Rank Correlation Coefficient			Intraclass Correlation Coefficient			Bland Altman		
		Mean Diff	LoA	Cov [%]	r	p	Mean Diff	Mean Diff	Mean	LoA	Cov [%]	r	p
Absolute Helicity [ $\text{m} \cdot \text{s}^{-2} \cdot \text{mL}^{-1}$ ]													
AoR	1	621	1,878	27	0.94	<0.01	0.84	58	397	7	0.95	<0.01	0.96
	2	851	2,432	37	0.87	<0.01	0.72	-77	1,147	21	0.69	<0.01	0.72
	3	231	663	11	0.97	<0.01	0.96	-135	1,148	21	0.7	<0.01	0.73
pAA	1	-70	500	12	0.97	<0.01	0.98	-216	547	12	0.93	<0.01	0.94
	2	-88	808	20	0.95	<0.01	0.94	13	758	18	0.85	<0.01	0.88
	3	-18	578	14	0.98	<0.01	0.97	229	624	14	0.89	<0.01	0.92
dAA	1	9	155	7	0.99	<0.01	0.99	29	112	5	0.99	<0.01	1.00
	2	37	146	7	0.99	<0.01	0.99	31	147	6	0.97	<0.01	1.00
	3	28	155	7	1.00	<0.01	0.99	2	157	7	0.96	<0.01	0.99
AoA	1	-23	140	6	0.99	<0.01	0.99	-26	137	4	0.99	<0.01	1.00
	2	-32	127	5	0.99	<0.01	0.99	49	262	9	0.97	<0.01	0.99
	3	-10	143	6	0.99	<0.01	0.99	74	259	8	0.98	<0.01	0.99
pDA	1	-71	216	6	0.99	<0.01	0.99	-13	293	6	1.0	<0.01	1.00
	2	-36	147	4	1.00	<0.01	1.00	24	287	6	0.97	<0.01	1.00
	3	35	162	4	1.00	<0.01	1.00	38	421	8	0.97	<0.01	0.99
dDA	1	34	139	5	0.99	<0.01	1.00	75	379	10	0.98	<0.01	0.98
	2	4	129	4	0.99	<0.01	1.00	60	269	7	0.97	<0.01	0.99
	3	-30	127	4	0.99	<0.01	1.00	-14	371	10	0.98	<0.01	0.99

Supplemental Table S4. Continued

Seg	Cohort	Training cohort						Validation cohort					
		Bland-Altman			Spearman Rank Correlation Coefficient			Bland-Altman			Spearman Rank Correlation Coefficient		
		Analysis	Mean Diff	LoA	Cov [%]	r	p	Mean Diff	Mean	Diff	LoA	Cov [%]	r
Absolute Local Normalized Helicity Volume [mL]													
AoR	1	1.1	8.1	25	0.81	<0.01	0.84	3.4	8.2	20	0.92	<0.01	0.88
	2	3.5	15.2	50	0.41	<0.01	0.30	7.4	8.6	23	0.92	<0.01	0.86
	3	2.4	11.4	39	0.46	<0.01	0.43	3.9	7.1	21	0.89	<0.01	0.86
pAA	1	1.9	5.0	10	0.93	<0.01	0.93	-1.4	3.9	8	0.92	<0.01	0.95
	2	-2.3	6.4	12	0.90	<0.01	0.88	-1.9	7.0	15	0.91	<0.01	0.88
	3	-4.2	6.5	12	0.90	<0.01	0.88	-0.5	8.0	16	0.85	<0.01	0.83
dAA	1	0.1	6.4	17	0.92	<0.01	0.93	-1.7	4.8	15	0.94	<0.01	0.95
	2	-1.2	6.8	17	0.93	<0.01	0.92	-1.8	4.9	16	0.92	<0.01	0.96
	3	-1.3	5.0	13	0.95	<0.01	0.95	-0.1	5.4	17	0.97	<0.01	0.95
AoA	1	-4.3	5.6	20	0.85	<0.01	0.92	-1.3	2.0	10	0.96	<0.01	0.96
	2	-0.0	2.6	11	0.93	<0.01	0.98	-0.4	4.1	21	0.89	<0.01	0.88
	3	4.2	3.5	12	0.97	<0.01	0.96	0.9	3.3	16	0.94	<0.01	0.93
pDA	1	2.0	2.8	10	0.96	<0.01	0.97	1.2	3.4	12	0.89	<0.01	0.95
	2	1.3	2.5	8	0.96	<0.01	0.97	0.7	4.0	14	0.9	<0.01	0.93
	3	-0.7	3.8	14	0.92	<0.01	0.95	-0.4	3.7	13	0.92	<0.01	0.94
dDA	1	2.7	3.5	11	0.92	<0.01	0.92	1.2	3.0	10	0.89	<0.01	0.94
	2	2.2	2.1	6	0.98	<0.01	0.98	1.6	4.5	15	0.85	<0.01	0.88
	3	-0.5	4.0	13	0.93	<0.01	0.91	0.3	4.4	15	0.89	<0.01	0.87

Supplemental Table S4. Continued

Seg	Analysis	Training cohort						Validation cohort					
		Bland-Altman			Spearman Rank Correlation Coefficient			Bland-Altman			Spearman Rank Correlation Coefficient		
		Mean Diff	Cov [%]	r	p	Mean Diff	Correlation Coefficient	Mean	Diff	LoA	Cov [%]	r	p
Volume [mL]													
AoR	1	3.1	17.3	24	0.79	0.82	8.6	16.6	20	0.87	<0.01	0.85	
	2	9.3	31.8	47	0.34	0.02	0.27	15.0	17.0	22	0.95	<0.01	0.85
	3	6.1	23.1	36	0.36	0.01	0.41	6.4	13.8	20	0.88	<0.01	0.84
pAA	1	3.5	12.8	13	0.72	<0.01	0.87	-3.8	9.9	10	0.95	<0.01	0.93
	2	-5.6	16.8	15	0.78	<0.01	0.76	-3.6	10.7	11	0.96	<0.01	0.93
	3	-9.2	14.3	14	0.80	<0.01	0.81	0.2	12.9	13	0.88	<0.01	0.88
dAA	1	4.0	11.9	13	0.87	<0.01	0.91	-1.9	7.5	10	0.95	<0.01	0.95
	2	0.4	11.5	13	0.90	<0.01	0.91	-2.7	6.7	9	0.97	<0.01	0.97
	3	-3.6	11.6	13	0.79	<0.01	0.89	-0.8	8.8	11	0.98	<0.01	0.94
AoA	1	-10.4	14.4	20	0.70	<0.01	0.72	-2.6	4.0	8	0.88	<0.01	0.93
	2	-0.0	7.3	12	0.91	<0.01	0.91	-2.2	5.9	12	0.96	<0.01	0.91
	3	10.4	8.7	12	0.9	<0.01	0.88	0.4	6.6	13	0.91	<0.01	0.88
pDA	1	4.5	6.2	9	0.91	<0.01	0.95	3.2	8.1	12	0.84	<0.01	0.93
	2	3.7	4.5	6	0.98	<0.01	0.97	2.1	7.4	11	0.89	<0.01	0.95
	3	-0.8	8.0	12	0.93	<0.01	0.92	-1.1	5.8	9	0.95	<0.01	0.97
dDA	1	4.2	4.6	7	0.9	<0.01	0.95	2.6	5.5	10	0.98	<0.01	0.96
	2	3.6	3.6	6	0.88	<0.01	0.97	2.5	5.3	9	0.98	<0.01	0.97
	3	-0.5	5.6	10	0.97	<0.01	0.94	-0.1	5.6	10	0.97	<0.01	0.96

Supplemental Table S4. Continued

Seg	Cohort	Training cohort						Validation cohort								
		Bland-Altman			Spearman Rank Correlation Coefficient			Intraclass Correlation Coefficient			Bland-Altman			Spearman Rank Correlation Coefficient		
		Analysis	Mean Diff	LoA	Cov [%]	r	p	Mean Diff	Mean	Diff	LoA	Cov [%]	r	p	Mean Diff	Mean
Centerline Length [mm]																
AoR	1	5.8	10.9	20	0.47	<0.01		0.59	6.9	10.0	18	0.68	<0.01		0.64	
	2	12.6	16.9	36	0.06	0.66	0.02	11.4	9.5	19	0.80	<0.01		0.69		
	3	6.7	14.4	35	0.15	0.31	0.10	4.6	8.5	19	0.59	<0.01		0.55		
pAA	1	3.9	10.7	14	0.36	0.01	0.18	-1.8	6.2	8	0.93	<0.01		0.84		
	2	-1.0	9.2	11	0.39	<0.01	0.30	1.1	6.2	8	0.81	<0.01		0.83		
	3	-4.9	6.5	8	0.63	<0.01	0.60	2.9	6.2	8	0.73	<0.01		0.81		
dAA	1	4.8	11.3	14	0.25	0.08	0.17	-1.7	5.6	7	0.87	<0.01		0.87		
	2	-0.8	10.3	12	0.31	0.03	0.26	0.5	5.1	7	0.85	<0.01		0.89		
	3	-5.6	7.4	9	0.51	<0.01	0.47	2.2	4.6	6	0.81	<0.01		0.88		
AoA	1	-14.5	14.6	16	0.19	0.18	0.31	-5.8	4.7	6	0.77	<0.01		0.72		
	2	-3.0	9.3	12	0.71	<0.01	0.72	-1.6	6.9	10	0.66	<0.01		0.53		
	3	11.5	7.2	8	0.71	<0.01	0.78	4.2	7.3	10	0.57	<0.01		0.50		
pDA	1	7.3	9.7	8	0.68	<0.01	0.78	2.1	12.7	10	0.74	<0.01		0.82		
	2	3.1	11.1	9	0.66	<0.01	0.70	4.5	12.5	10	0.82	<0.01		0.85		
	3	-4.3	13.7	12	0.49	<0.01	0.54	2.5	9.9	8	0.83	<0.01		0.88		
dDA	1	7.4	8.2	7	0.87	<0.01	0.83	1.7	11.6	9	0.77	<0.01		0.84		
	2	3.3	10.5	8	0.68	<0.01	0.75	5.1	10.9	9	0.84	<0.01		0.89		
	3	-4.1	12.2	10	0.54	<0.01	0.57	3.4	9.1	8	0.89	<0.01		0.90		

Supplemental Table S4. Continued

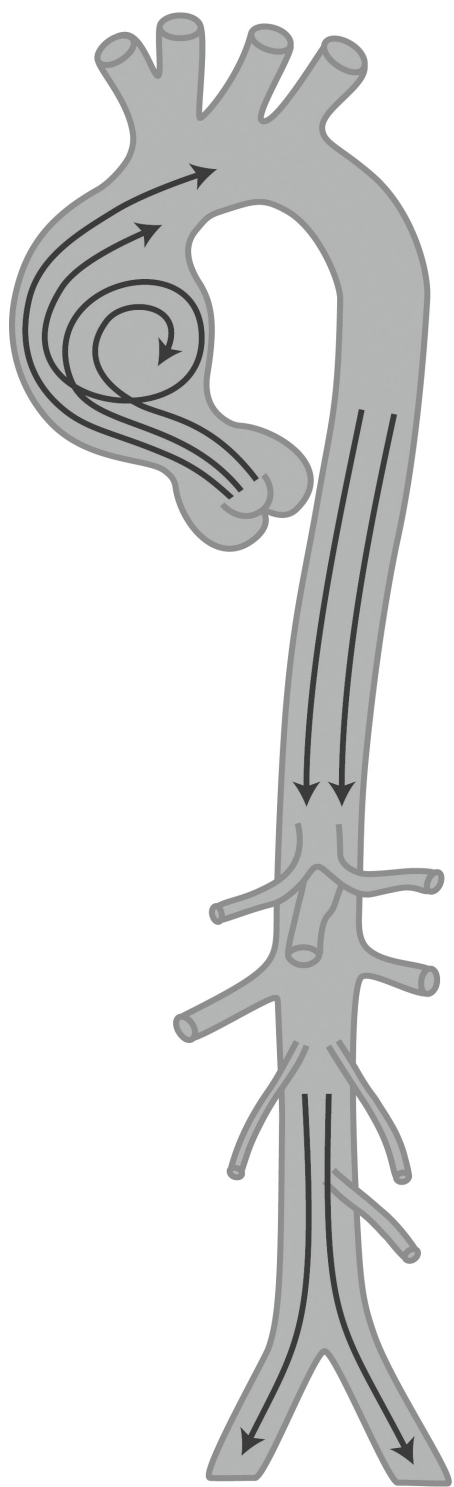
Seg	Analysis	Training cohort						Validation cohort					
		Bland-Altman			Spearman Rank Correlation Coefficient			Intraclass Correlation Coefficient			Bland-Altman		
		Mean Diff	LoA	Cov [%]	r	p	Mean Diff	Mean Diff	Mean Diff	Mean	LoA	Cov [%]	Spearman Rank Correlation Coefficient
Maximal Diameter [mm]													
AoR	1	-1.2	6.1	7	0.91	<0.01	0.86	0.0	3.8	4	0.94	<0.01	0.95
	2	-5.7	10.7	11	0.65	<0.01	0.51	-0.7	3.5	4	0.92	<0.01	0.96
	3	-4.5	7.4	8	0.65	<0.01	0.62	-0.7	3.1	3	0.93	<0.01	0.96
pAA	1	-0.3	5.1	6	0.84	<0.01	0.80	-1.9	6.6	8	0.23	0.11	0.34
	2	-4.4	10.7	12	0.08	0.58	0.08	-3.2	7.6	9	0.46	<0.01	0.54
	3	-4.1	9.3	10	0.31	0.03	0.36	-1.2	7.2	8	0.56	<0.01	0.46
dAA	1	-0.0	2.3	3	0.95	<0.01	0.98	-0.0	2.4	3	0.95	<0.01	0.96
	2	0.5	2.2	3	0.95	<0.01	0.98	-1.2	5.7	7	0.93	<0.01	0.87
	3	0.5	2.3	3	0.94	<0.01	0.98	-1.1	5.3	7	0.97	<0.01	0.89
AoA	1	-0.2	3.6	5	0.92	<0.01	0.91	-0.0	1.7	3	0.96	<0.01	0.96
	2	0.4	3.4	5	0.91	<0.01	0.92	-0.5	2.7	4	0.98	<0.01	0.93
	3	0.6	2.5	4	0.86	<0.01	0.95	-0.5	2.5	4	0.98	<0.01	0.94
pDA	1	1.5	2.0	3	0.88	<0.01	0.94	1.1	1.9	3	0.96	<0.01	0.93
	2	1.3	1.7	3	0.86	<0.01	0.96	0.1	1.2	2	0.95	<0.01	0.98
	3	-0.2	1.1	2	0.98	<0.01	0.98	-1.0	1.2	2	0.97	<0.01	0.97
dDA	1	0.7	1.6	3	0.91	<0.01	0.96	0.8	2.5	5	0.76	<0.01	0.89
	2	1.2	2.1	4	0.83	<0.01	0.93	0.3	2.7	5	0.89	<0.01	0.92
	3	0.4	1.8	3	0.90	<0.01	0.94	-0.5	3.3	7	0.84	<0.01	0.85

Supplemental Table S4. Continued

Seg	Analysis	Cohort			Training cohort						Validation cohort					
		Bland-Altman			Spearman Rank Correlation Coefficient			Intraclass Correlation Coefficient			Bland-Altman			Spearman Rank Correlation Coefficient		
		Mean Diff	LoA	COV [%]	r	p	Mean Diff	Mean Diff	Mean Diff	Mean Diff	LoA	COV [%]	r	p	ICC	Intraclass Correlation Coefficient
Curvature Radius [mm]																
AoR	1	1.6	66.6	54	0.32	0.02	0.41	5.8	72.1	66	0.40	<.01	0.31			
	2	-58.3	342.8	188	-0.02	0.88	0.02	19.5	60.1	63	0.35	0.01	0.26			
	3	-59.9	337.2	186	0.24	0.09	0.05	13.7	55.4	62	0.13	0.38	0.09			
pAA	1	-1.6	20.3	25	0.45	<.01	0.22	-3.2	20.4	25	0.40	<.01	0.24			
	2	-4.7	18.2	21	0.44	<.01	0.44	0.5	14.4	18	0.29	0.04	0.17			
	3	-3.0	15.5	18	0.67	<.01	0.66	3.7	16.5	20	0.37	0.01	0.39			
dAA	1	4.6	26.0	23	0.73	<.01	0.71	3.2	10.6	11	0.82	<.01	0.78			
	2	2.3	26.4	23	0.66	<.01	0.73	0.2	12.8	13	0.72	<.01	0.78			
	3	-2.4	16.4	15	0.92	<.01	0.90	-2.9	14.2	15	0.63	<.01	0.64			
AoA	1	1.5	14.7	16	0.72	<.01	0.74	4.0	23.3	20	0.9	<.01	0.87			
	2	-3.6	16.4	17	0.79	<.01	0.81	-2.1	29.6	24	0.86	<.01	0.83			
	3	-5.1	18.4	20	0.8	<.01	0.7	-6.2	30.9	26	0.85	<.01	0.78			
pDA	1	-1.8	14.4	14	0.87	<.01	0.77	-0.8	8.3	10	0.76	<.01	0.75			
	2	2.3	14.5	15	0.84	<.01	0.75	2.5	9.0	11	0.79	<.01	0.74			
	3	4.1	9.5	10	0.92	<.01	0.92	3.3	3.9	5	0.9	<.01	0.93			
dDA	1	8.9	60.8	21	0.86	<.01	0.89	-25.3	63.4	21	0.92	<.01	0.90			
	2	7.3	59.3	21	0.77	<.01	0.91	1.1	68.3	24	0.87	<.01	0.87			
	3	-1.6	42.9	16	0.78	<.01	0.93	26.4	63.7	21	0.85	<.01	0.92			

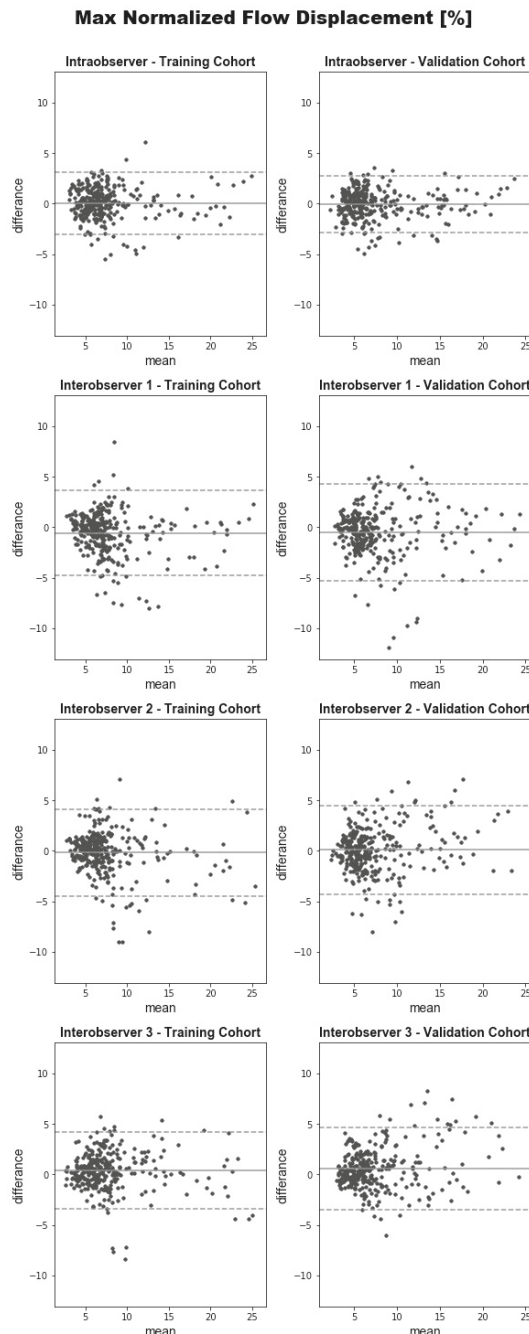
Characteristics are presented per anatomical segment over all subjects and systolic phases ( $n = 60$ ). Abbreviations: Mean Diff – mean difference, LoA – limits of agreement ( $1.96 \times$  standard deviation difference), COV – coefficient of variation, ICC – intraclass correlation coefficient, WSS – wall shear stress, AoR – aortic root, pAA – proximal ascending aorta, dAA – distal ascending aorta, pDA – aortic arch, AoA – distal descending aorta, and dDA – distal descending aorta.



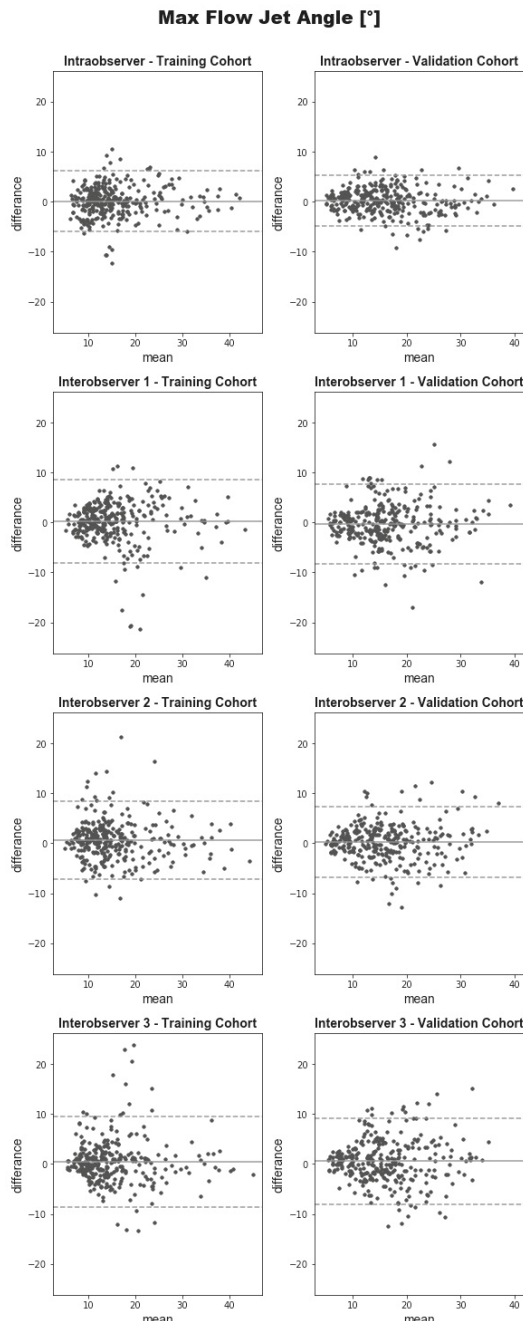


# Supplemental Figures to Chapter 3

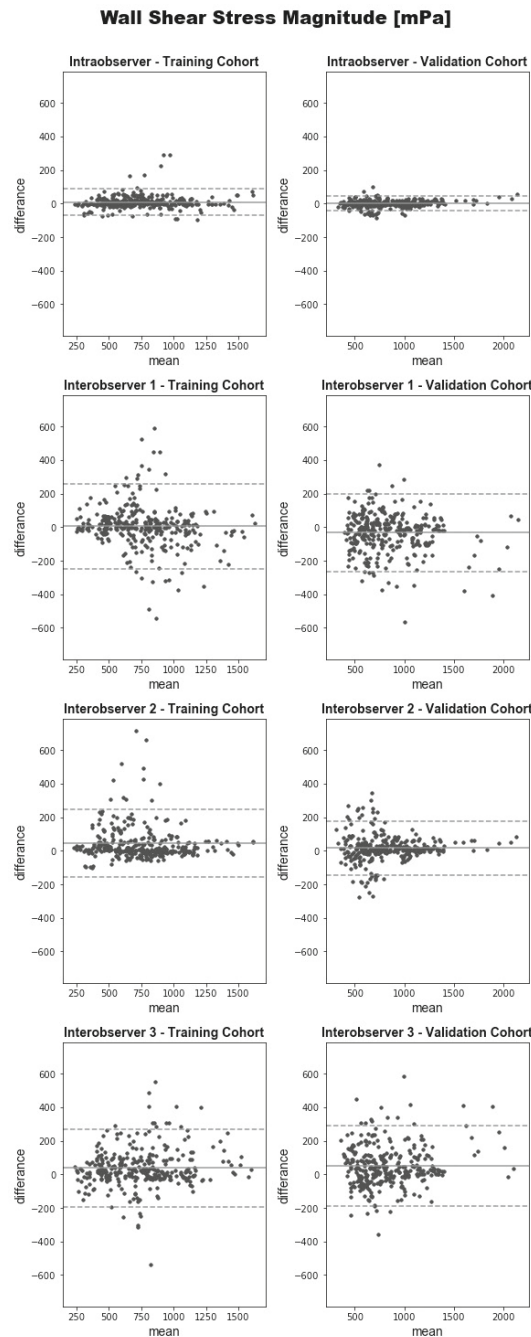
---



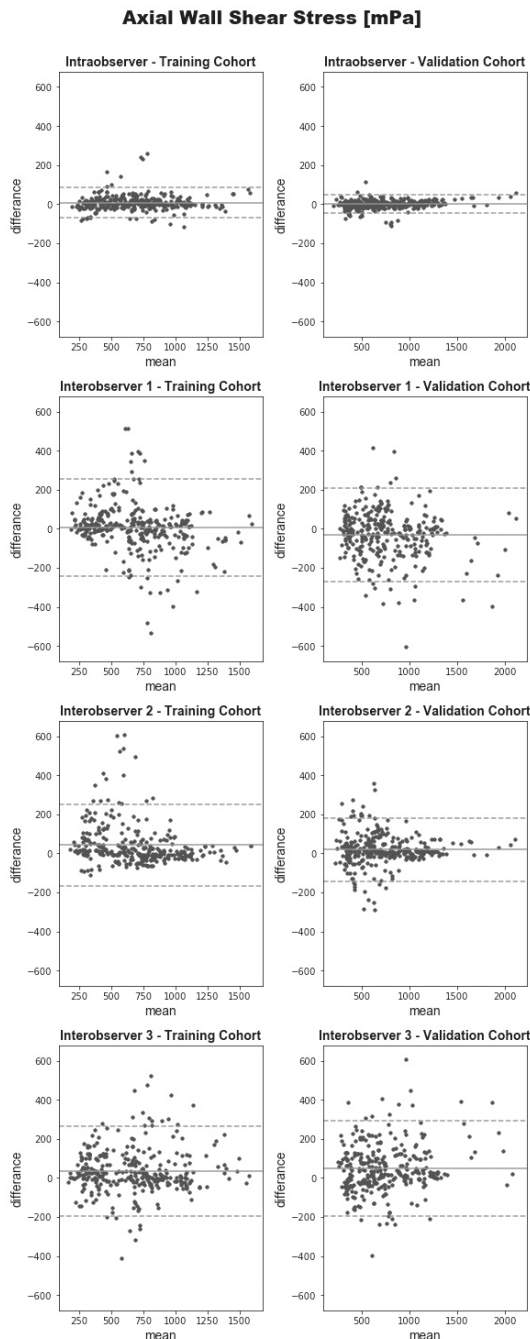
**Supplemental Figure S1.** Bland-Altman plots for the normalized flow displacement. Plots demonstrate the results per cohort over all subjects, anatomical segments and systolic phases ( $n=300$ ). Displayed on the vertical and horizontal axis, the differences and means, respectively, in %. Horizontal lines show mean differences (Diff, solid line) and the limits of agreement (LoA, dashed lines).



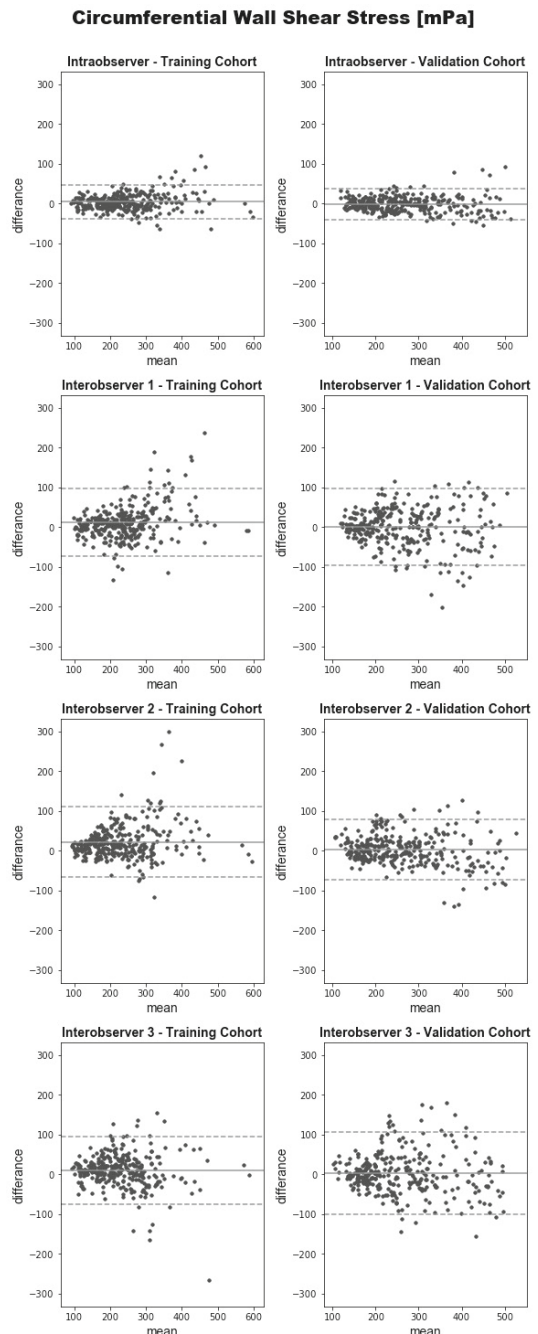
**Supplemental Figure S2.** Bland-Altman plots for the flow jet angle. Plots demonstrate the results per cohort over all subjects, anatomical segments and systolic phases ( $n=300$ ). Displayed on the vertical and horizontal axis, the differences and means, respectively, in degree. Horizontal lines show mean differences (Diff, solid line) and the limits of agreement (LoA, dashed lines).



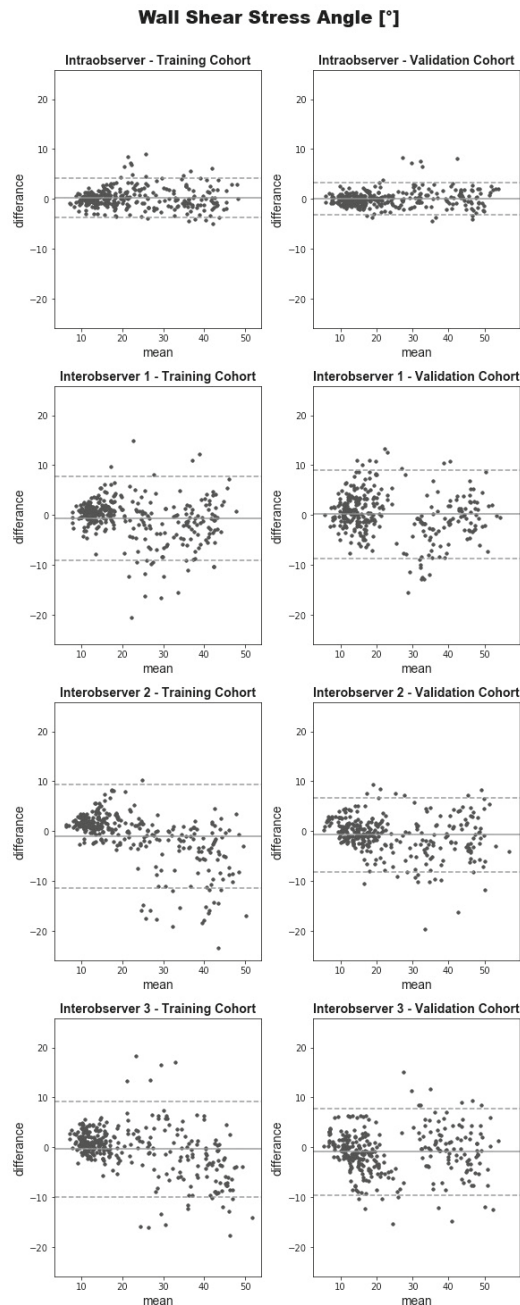
**Supplemental Figure S3.** Bland-Altman plots for the wall shear stress magnitude. Plots demonstrate the results per cohort over all subjects, anatomical segments and systolic phases ( $n=300$ ). Displayed on the vertical and horizontal axis, the differences and means, respectively, in mPa. Horizontal lines show mean differences (Diff, solid line) and the limits of agreement (LoA, dashed lines).



**Supplemental Figure S4.** Bland-Altman plots for the axial wall shear stress. Plots demonstrate the results per cohort over all subjects, anatomical segments and systolic phases ( $n=300$ ). Displayed on the vertical and horizontal axis, the differences and means, respectively, in mPa. Horizontal lines show mean differences (Diff, solid line) and the limits of agreement (LoA, dashed lines).

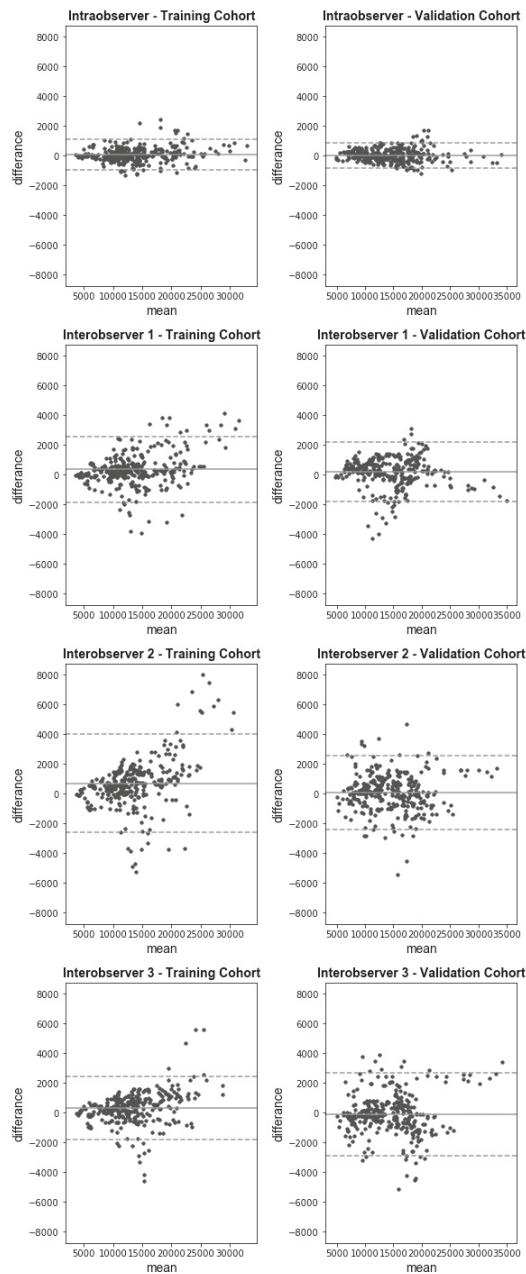


**Supplemental Figure S5.** Bland-Altman plots for the circumferential wall shear stress. Plots demonstrate the results per cohort over all subjects, anatomical segments and systolic phases ( $n=300$ ). Displayed on the vertical and horizontal axis, the differences and means, respectively, in mPa. Horizontal lines show mean differences (Diff, solid line) and the limits of agreement (LoA, dashed lines).

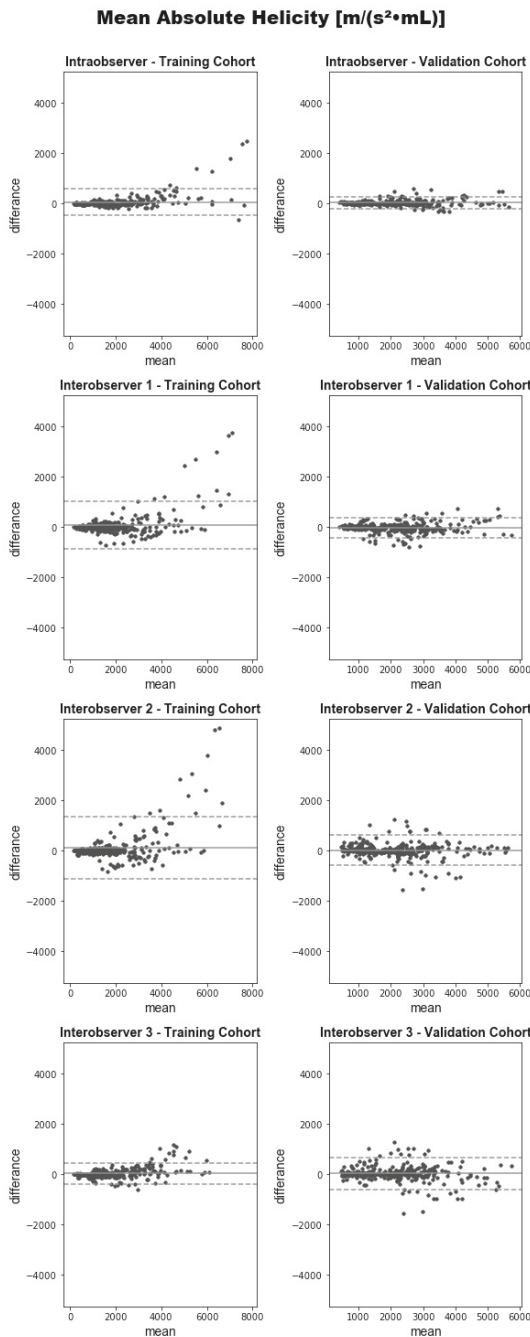


**Supplemental Figure S6.** Bland-Altman plots for the wall shear stress angle. Plots demonstrate the results per cohort over all subjects, anatomical segments and systolic phases ( $n=300$ ). Displayed on the vertical and horizontal axis, the differences and means, respectively, in degree. Horizontal lines show mean differences (Diff, solid line) and the limits of agreement (LoA, dashed lines).

### Mean Vorticity Norm [ $1/(s \cdot mL)$ ]

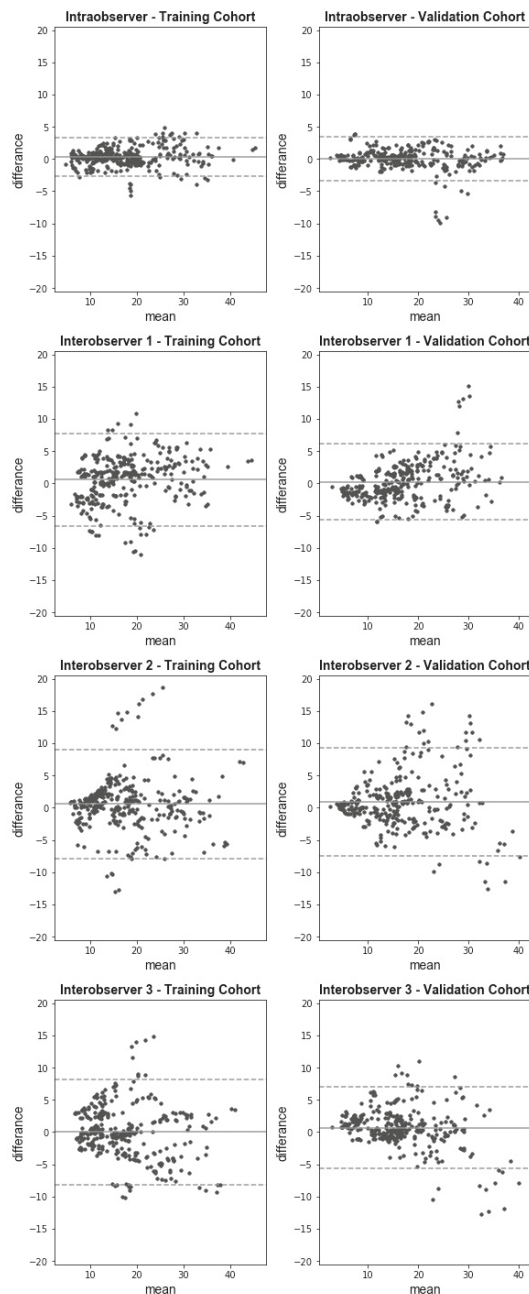


**Supplemental Figure S7.** Bland-Altman plots for the vorticity norm. Plots demonstrate the results per cohort over all subjects, anatomical segments and systolic phases ( $n=300$ ). Displayed on the vertical and horizontal axis, the differences and means, respectively, in  $s^{-1} \cdot mL^{-1}$ . Horizontal lines show mean differences (Diff, solid line) and the limits of agreement (LoA, dashed lines).

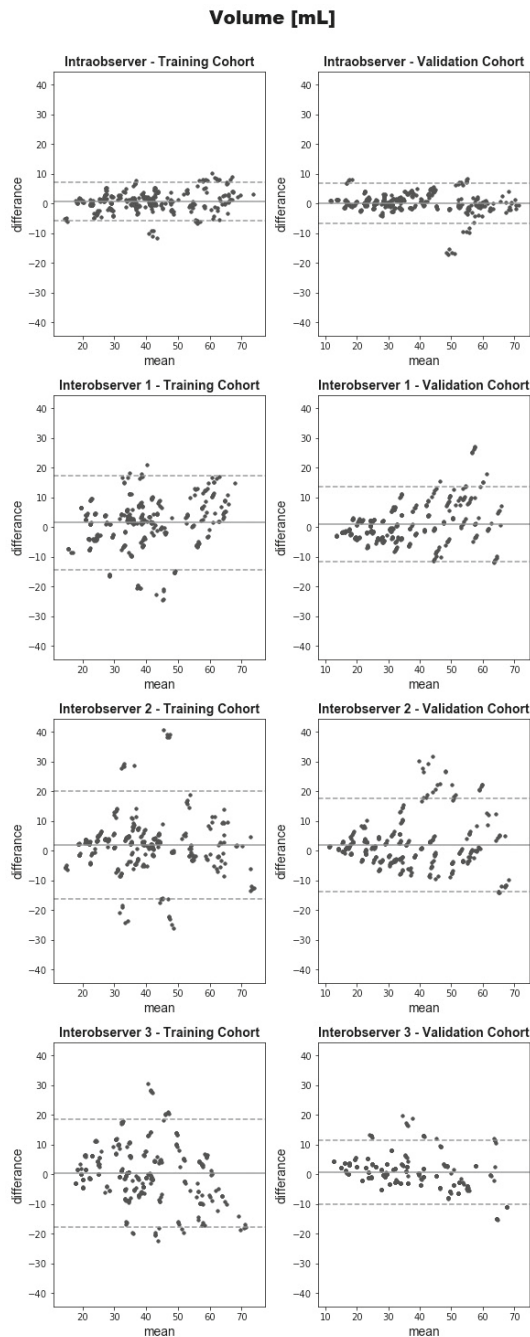


**Supplemental Figure S8.** Bland-Altman plots for the absolute helicity. Plots demonstrate the results per cohort over all subjects, anatomical segments and systolic phases ( $n=300$ ). Displayed on the vertical and horizontal axis, the differences and means, respectively, in  $\text{m} \cdot \text{s}^{-2} \cdot \text{mL}^{-1}$ . Horizontal lines show mean differences (Diff, solid line) and the limits of agreement (LoA, dashed lines).

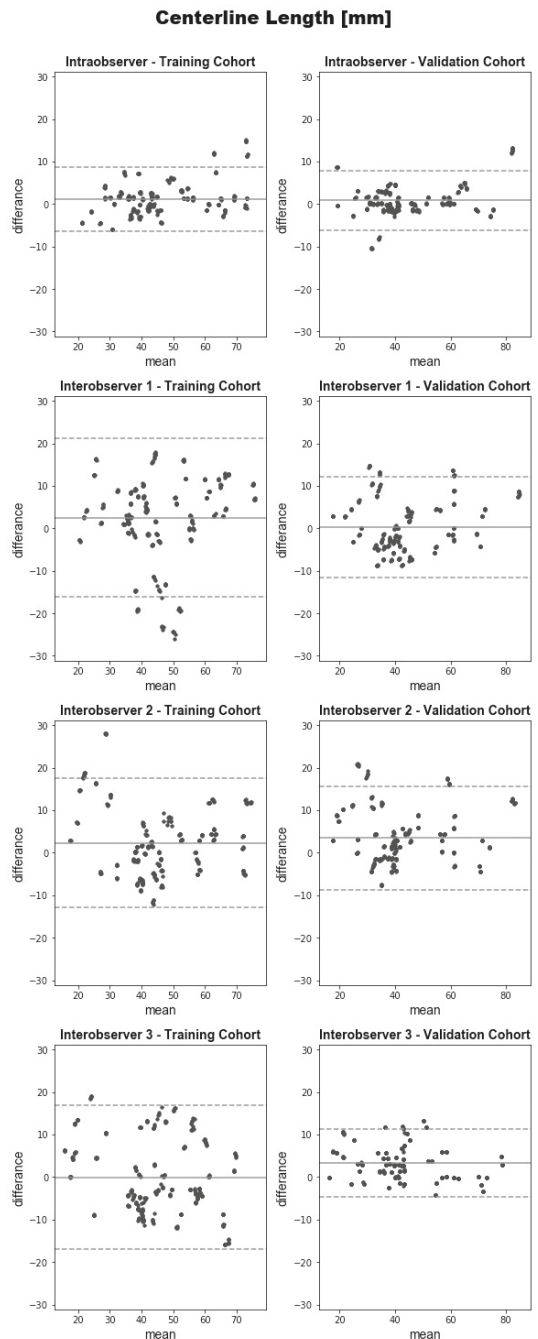
### Absolute Local Normalized Helicity Volume [mL]



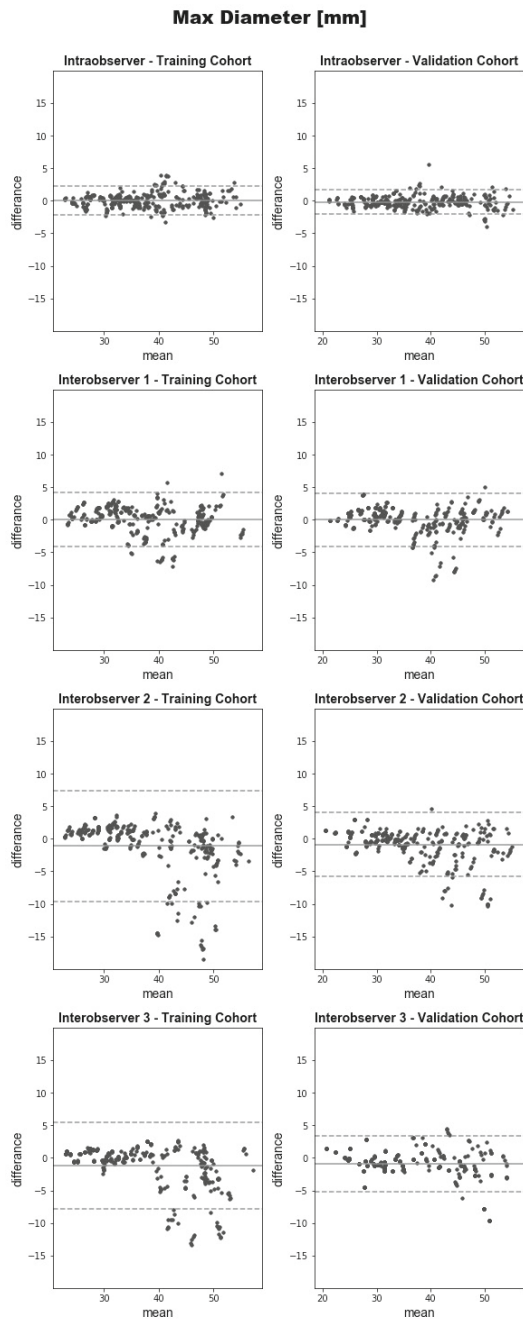
**Supplemental Figure S9.** Bland-Altman plots for the absolute local normalized helicity volume. Plots demonstrate the results per cohort over all subjects, anatomical segments and systolic phases ( $n=300$ ). Displayed on the vertical and horizontal axis, the differences and means, respectively, in mL. Horizontal lines show mean differences (Diff, solid line) and the limits of agreement (LoA, dashed lines).



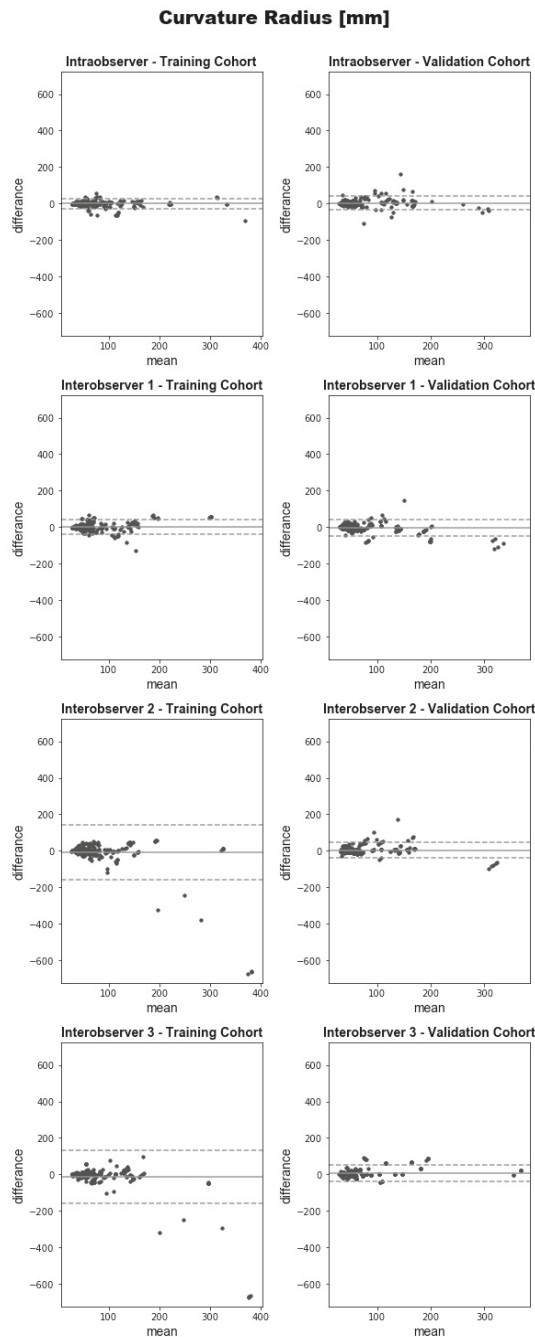
**Supplemental Figure S10.** Bland-Altman plots for the volume. Plots demonstrate the results per cohort over all subjects, anatomical segments and systolic phases ( $n=300$ ). Displayed on the vertical and horizontal axis, the differences and means, respectively, in mL. Horizontal lines show mean differences (Diff, solid line) and the limits of agreement (LoA, dashed lines).



**Supplemental Figure S11.** Bland-Altman plots for the centerline length. Plots demonstrate the results per cohort over all subjects, anatomical segments and systolic phases ( $n=300$ ). Displayed on the vertical and horizontal axis, the differences and means, respectively, in mm. Horizontal lines show mean differences (Diff, solid line) and the limits of agreement (LoA, dashed lines).



**Supplemental Figure S12.** Bland-Altman plots for the maximal diameter. Plots demonstrate the results per cohort over all subjects, anatomical segments and systolic phases (n=300). Displayed on the vertical and horizontal axis, the differences and means, respectively, in mm. Horizontal lines show mean differences (Diff, solid line) and the limits of agreement (LoA, dashed lines).



**Supplemental Figure S13.** Bland-Altman plots for the curvature radius. Plots demonstrate the results per cohort over all subjects, anatomical segments and systolic phases ( $n=300$ ). Displayed on the vertical and horizontal axis, the differences and means, respectively, in mm. Horizontal lines show mean differences (Diff, solid line) and the limits of agreement (LoA, dashed lines).

